WAVE PROPAGATION IN ANISOTROPIC ROCKS

Annual Technical Report Number 1
Contract No. H0210022
Sponsored by Advanced Research Projects
Agency, ARPA Order No. 1579, Amend. 2
Program Code 1F10

Principal Investigator: Dr. W. Goldsmith
Associate Investigator: Dr. J.L. Sackman
University of California
Berkeley, California 94720

Unclassified
Security Classification

3200.8 (Att 1 to Encl 1)
Mar 7, 66

DOCUMENT CONTROL DATA - R & D
(Security classification of title, body of abstract and indexing annotation must be entered when the overall report is classified)

1. ORIGINATING ACTIVITY (Corporate author)
University of California, Berkeley

2a. REPORT SECURITY CLASSIFICATION
Unclassified

2b. GROUP

3. REPORT TITLE
WAVE PROPAGATION IN ANISOTROPIC ROCKS

4. DESCRIPTIVE NOTES (Type of report and inclusive dates)
Annual Technical Report Number 1: February 5, 1971 to Feb. 4, 72

5. AUTHOR(S) (First name, middle initial, last name)
Werner Goldsmith and Jerome L. Sackman

6. REPORT DATE
March 3, 1972

7a. TOTAL NO. OF PAGES
90

7b. NO. OF REFS
21

8a. CONTRACT OR GRANT NO.
H0 210022

b. PROJECT NO.
ARPA Order No. 1579, Amend. 2

c. Program Code 1F10

d.

9a. ORIGINATOR'S REPORT NUMBER(S)
[redacted]

9b. OTHER REPORT NO(S) (Any other numbers that may be assigned this report)

10. DISTRIBUTION STATEMENT
Distribution of this document is unlimited

11. SUPPLEMENTARY NOTES

12. SPONSORING MILITARY ACTIVITY
Advanced Research Projects Agency

13. ABSTRACT
~~This~~ report presents the work of the first year on the contract involving (a) the detection of body and surface waves in blocks of Yule marble (b) the analysis of such pulses produced by impact using both integral transform and finite element methods, and (c) the determination of the static and dynamic properties of this material including fracture characteristics. In the first phase, satisfactory transducer packages have been constructed and embedment techniques are under development. Theoretically, displacement fields have been obtained from the integral transform method with the aid of the Cagniard-de Hoop technique. A finite element program written for the three-dimensional anisotropic case is being tested on the subject problem. Static stress-strain curves for single and repeated loading have been obtained for Yule marble. Techniques for the determination of the principal axes of the rock have been developed, and methods for evaluating the fracture strength of the rock under varying rates of strain are being perfected.

DD FORM 1 NOV 1473

Unclassified
Security Classification

14. KEY WORDS	LINK A		LINK B		LINK C	
	ROLE	WT	ROLE	WT	ROLE	WT
Rock Mechanics						
Properties of rock						
Fracture of rock						
Wave Propagation						
Anisotropic Half-spaces						
Impact						
Transient Signal Detection in Rocks						
Transducers						

ANNUAL TECHNICAL REPORT NUMBER ONE

ARPA Order Number: 1579, Amendment 2

Program Code Number: 1F10

Contractor: The Regents of the University of California

Effective Date of Contract: February 5, 1971

Contract Expiration Date: February 4, 1972

Amount of Contract: $60,000

Contract Number: H0210022

Principal Investigator: Professor W. Goldsmith, (415) 642-3739

Project Engineer: Professor J. L. Sackman, (415) 642-2950

Title: "Wave Propagation in Anisotropic Rocks"

Report Period: February 5, 1971 to February 4, 1972

Sponsored by

Advanced Research Projects Agency

ARPA Order No. 1579, Amend. 2

Program Code 1F10

This research was supported by the Advanced Research Projects Agency of the Department of Defense and was monitored by the Bureau of Mines under Contract No. H0210022.

TABLE OF CONTENTS

ABSTRACT

The following report defines the scope, provides a narration of the technical accomplishments and current status after one year of operation, and lists the work remaining to be done under U.S. Bureau of Mines Contract No. H0210022 with the University of California, Berkeley, on a project entitled, "Wave Propagation in Anisotropic Rocks." The project has been divided into three major phases, namely (a) an experimental examination of the wave processes in Yule marble blocks, (b) a theoretical study of the pulse propagation produced by a concentrated transient source normal to the surface of a homogeneous, elastic transversely isotropic semi-infinite solid using (1) an integral transform technique, and (2) a finite element method, and (c) a determination of the geometric and static and dynamic mechanical properties of the Yule marble, including fracture characteristics.

In the experimental wave propagation phase, the major accomplishments achieved to date include the development of a crystal transducer package with a laterally unconstrained crystal employed as a sensing element, the calibration of both the crystal and the entire package, the development of installation techniques for the embedment of the transducer inside cores drilled in rock bars, and some progress in the development of a suitable grouting material to fill the core holes after installation of the transducer unit with a minimum of dynamic mismatch. The integral transform technique has been developed and partially tested to obtain the displacement field in the transversely isotropic solid with an axis located in the free surface under a Heaviside input. This process constructs a three-dimensional solution from the integration of

a series of two-dimensional problems associated with line loads on the surface of the half-space. It employs a Cagniard-de Hoop transformation which simplifies the inversion process and leads to a physical interpretation of the transient wave process in terms of well-established concepts of wave and slowness surfaces that have been employed in the field of crystal acoustics.

A finite element program has been written for the three-dimensional problem cited above and is currently in the debugging and test phase. It has been specialized to the simpler case of isotropic behavior where other solutions for checking purposes exist. Results obtained to date include the uniaxial wave process in a rod and the surface motion of a half-space. They are very encouraging in terms of providing good correspondence with these other solutions, and indicate the immediate application of the program to the subject problem after some additional investigation of the numerical integration schemes.

Crystallographic techniques have been developed for the location of the axis of elastic symmetry of the Yule marble specimens. Static compressive tests, some with repeated loading, have been conducted on samples of the material, indicating significant non-linearities and the presence of hysteresis. A technique has been developed for the generation of constant strain rates in the intermediate range of 10 to 100 sec^{-1} utilizing an adaptation of a Hopkinson-bar procedure.

This work will be continued and, during the coming year, the various phases of the program will be intimately correlated. The program is on schedule and no major difficulties are anticipated in the completion of the work according to the original schedule.

PREFACE

This is the first annual report concerned with the technical activities performed under Contract No. H0210022 of the U.S. Bureau of Mines with the University of California on the subject entitled "Wave ropagation in Anisotropic Rocks." It covers the period from February 5, 1971 to Februar; 4, 1972 and will be followed by additional reports involving extensions of the present contract. The scope of the program is detailed in the proposal identified as UCB-Eng 3154, dated 19 August, 1970 and submitted on behalf of the University of California, Berkeley, by W. Goldsmith as Principal Investigator, and is also spelled out in Article I of the subject contract. It was envisioned initially that the completion of the entire investigation outlined in these documents would require a period somewhat in excess of two years; consequently, the present document comprises an interim rather than a terminal report of the program. The time schedule originally indicated for the various phases of the work has been closely observed.

The scope of the activities was subdivided into several categories as follows: (a) An experimental examination of the wave processes produced by impacts of spheres on the surface of large blocks of Yule marble, involving the measurement of surface and body waves by means of strain gages, accelerometers, and transducer packages embedded in the solid; (b) A theoretical analysis of the pulses produced in the block, modelled as a transversely anisotropic half-space, using integral transform and other mathematical techniques, and comparison of the predicted response of this model with experimental data; and (c) The examination of the mechanical properties of the material Yule marble.

including the effect of rate of loading on fracture properties. Each of four graduate students was assigned to a separate phase of the program: Mr. K. Krishnamoorthy devoted his efforts to part (a); Mr. S. L. Suh was concerned with the development and numerical evaluation of the analysis employing integral transform techniques; Mr. M. Katona occupied himself with the development, validation and application of a finite-element solution of the problem; and Mr. S. Howe was associated with the phase involving the determination of the mechanical properties of the rock including fracture. These students are utilizing the results of their efforts on this project in whole or in part for their doctoral dissertations or masters theses. Professor W. Goldsmith, Division of Applied Mechanics, and Professor J. L. Sackman, Division of Structural Engineering and Structural Mechanics, jointly supervised the entire program since its inception and are responsible for its conduct. Technical assistance in certain portions of the Fortran programming was rendered by Mr. R. Kenner, and the technical staff of the Departments of Mechanical Engineering, Civil Engineering and Geology and Geophysics assisted in the operation of the experimental investigation.

There have been no major technical difficulties in the pursuit of the original goals, and the progress made is encouraging to the point of predicting that these will be achieved within the original time span estimated. Some changes in emphasis or techniques may be required, particularly in the methodology of determining the strain-rate effects on the fracture process. Furthermore, an additional effort may be made to provide a sound mechanical model for the Yule marble. The program has already indicated the desirability of additional investigations in

the domain of anisotropic wave propagation that will be detailed in the appropriate section of the report. The program has exhausted the funds initially requested without any overrun.

I. INTRODUCTION

a) Historical Background

A detailed examination of the analysis of transients in homogeneous, anisotropically elastic media has been undertaken only during the last fifteen years[1-7]*, and specific numerical results have been obtained essentially only for two-dimensional classes of problems. One of these is the solution to the application of a time-dependent point load on the free surface of a quasi-isotropic half-space, i.e. a material in which there exists an axis of elastic symmetry perpendicular to the free surface, leading to an axisymmetric problem.[6] Another result has been recently obtained by Burridge[7] for a line load applied to the surface of a semi-infinite solid, with cubic symmetry, i.e. one where the axis of elastic symmetry lies in the free surface; this is also a two-dimensional problem, albeit of a different nature. In spite of the limited nature of the presently available theoretical development, there have been no corresponding experimental investigations whose results could be compared with the predictions of these theories.

As an initial attempt to broaden the scope of knowledge in this domain, a closely coordinated theoretical and experimental program was undertaken at the University of California by Dr. T. E. Ricketts that was concerned with the surface wave pulse propagation produced by normal impact of a sphere on a homogeneous, transversely anisotropic half-space.[8][9] For the experimental phase, this solid was modelled by a large block of Yule marble whose axis of elastic symmetry was

---

*Numbers in superiors refer to the Bibliography at the end of the report.

located in the free surface plane. Analytical expressions were obtained using a combined Laplace-Fourier transform method which provided the formal solution of the three-dimensional problem in transform space. The relations were derived for general anisotropy and then specialized for the transversely anisotropic case; with the elastic symmetry axis in the free surface however, a complete inversion of the displacement field into the real time-space domain was not obtained.

The experiment utilized 3/4" diameter steel spheres which struck the test block at impact velocities of about 20 ft/sec. Semi-conductor strain gages and specially-fabricated quartz crystal accelerometers were employed to detect the horizontal and vertical components of the disturbance, respectively. The former were mounted both along and normal to radial lines drawn from the impact point in order to detect any quasi-Rayleigh components.

The experimental procedure provided surface wave group velocity, group slowness, amplitude and attenuation curves for the Yule marble. The experimental slowness curve was compared to the corresponding analytical phase and group slowness curves computed using both static and dynamic properties of this substance which were determined in this study. A comparison of analytical and experimental results provided acceptable correlation.

The investigation described above represented the first combined analytical and experimental program involving transient response of any anisotropic elastic solid and also the first to consider a fully three-dimensional problem. This pioneering effort was successful, but of necessity of limited scope, providing basic features of the solution

applicable to surface wave phenomena. Details of the body wave motion were not obtained, but the work represents a foundation for future investigations and served as the motivation for the scope of the current contract.

b) Scope of the Research Proposed Under Contract No. H0210022

The purpose of the investigation was the determination of the response of a real rock material to a surface impact. To this end, the variation of stresses in the interior and on the surface of a block of Yule marble to transient loading by a spherical projectile were to be measured and compared to a corresponding mathematical model of the system.

Two large blocks of Yule marble were supplied by the U.S. Bureau of Mines for testing purposes. This material was selected since it represents a reasonably homogeneous continuum on the scale of the wavelengths employed, yet exhibits a greater degree of transverse anisotropy than any other natural substance available in the required size and quality. In one of the blocks, the axis of elastic symmetry is in one of the free surfaces, but not parallel to the edges; consequently, the block can be used either as a transversely isotropic solid loaded in a direction parallel to one of the non-symmetric axes or at an angle to these. To be employed in an experiment involving a quasi-isotropic situation, it would be necessary to machine the block so as to produce a loading plane perpendicular to the axis of elastic symmetry.

The methodology for the measurement of surface phenomena has been satisfactorily worked out by Ricketts utilizing semi-conductor strain

gages and accelerometers[8]. The present objective requires the development and installation of transducers capable of recording the response in various directions in the interior of the block. To this effect, it was necessary to institute a developmental program for the manufacture, calibration and installation of minute sensor packages to be placed at the terminus of various holes of very small diameter relative to the block size. In addition to the actual problems of excavation, there is the crucial problem of selection of a suitable filler material that anchors the transducer package, completely fills the drill hole and exhibits appropriate acoustic impedance and other mechanical characteristics compatible with the parent material. The proper functioning of the externally calibrated transducer unit in situ will require a special investigative subprogram and constant attention.

In view of the limited space available for the placement of the transducers, their locations within the block must be selected with great care so as to permit the recording of data for a wide variety of external loading situations and for different response quantities, taking full advantage of the symmetry of the block. Loading will occur by means of sphere impacts using either a drop or pneumatic techniques; the initial and terminal velocities will be monitored so as to permit control of the characteristics of the incident impulse.

The mathematical model employed in this study consists of a transversely isotropic homogeneous elastic half-space subjected to a transient point load applied normal to the free surface that contains the axis of elastic symmetry. The integral transform techniques initiated in References (8) and (9) were to be further developed so as to permit

numerical evaluation using high-speed digital computing equipment of required field variables at selected stations. During this process, it was found to be necessary to employ a different transformation than sketched earlier in order to obtain a more practical solution algorithm. Eventually, the displacement and stress fields are to be generated from this analysis for arbitrary loading histories.

It was deemed necessary to initiate an independent method of analysis involving the discretization of the block by means of the finite element method coupled with a variational principle from which the equations of motion are derived. This technique will be used to validate the results obtained from the integral transform procedure and has a potential for broader applications in the theoretical investigation of more general wave propagation processes such as might be encountered in the field. These complications might include the effects of total anisotropy, inhomogeneity, the presence of boundaries, more general loading conditions, and possibly inelastic behavior. This effort has paid unanticipated dividends by both providing a degree of confidence in the transform approach upon successful correlation of corresponding numerical results, and by indicating the direction to be followed analytically in the pursuit of the solution of more complicated phenomena beyond the scope of the present contract.

In order to predict with confidence the diverse phenomena expected to occur upon loading of this material, it is crucial that a full knowledge of the complete mechanical behavior and its dependence upon loading rate as well as the orientation of the axes of elastic symmetry within the two actual blocks be precisely delineated. Some information

on the values of the static and dynamic elastic constants as well as the orientation of the principal axes for one of the blocks was indicated in Reference (8); however, the precision of the numerical procedures to be employed in the analysis requires a verification and refinement of these values as well as a more extensive investigation of the stress, strain, strain-rate behavior of the material composing both blocks. In addition, the effect of loading rate on the fracture characteristics of the material was to be determined so as to determine the limits of applicability of the analysis detailed above. The data will be employed to construct a physical model of the behavior pattern of the Yule marble that might be useful in assessing the deficiencies of the homogeneous linearly elastic comportment assumed in the mathematical treatment of the impact phenomenon, as well as being of considerable value in its own right.

Stress-strain curves for the marble have been obtained at various low rates of loading and for repeated loading below the failure point. Methods of achieving higher loading rates have been investigated and will be applied. A technique for the determination of fracture characteristics of bone[10] will be utilized for the corresponding investigation of the marble, supplemented by suitable visual techniques.

A significant portion of the total effort was devoted to the evolution and development of new techniques necessary to achieve both the experimental and numerical objectives of the program. This has involved the selection, design, construction and calibration of the transducer package, the methodology of drilling and the fabrication and injection of filler material for the holes. Further, this includes the writing

and debugging of the computer programs and their specialization to problems with known solutions for the purpose of validation. Investigation of possible methods of determining the principal axes of the blocks with sufficient accuracy, yet reasonable in terms of cost and time expenditure, have received special attention. These and other required preliminary efforts do not manifest themselves in immediate concrete results, but are vitally necessary to the successful execution of the project.

c) Current Status of the Project

After one year of operation, the accomplishments of the project correspond quite closely to those anticipated in the program schedule of the original proposal. The transducer development, budgeted at six months, has been completed and a calibration procedure standardized. Installation techniques, including coring methods and investigation of filler materials, are still in the process of examination, although the majority of the effort for this phase has been expended. When this task is completed, expected to occur in another two to three months, locations of the transducers in the two Yule marble blocks together with access holes will be selected and in situ calibration and testing will be initiated.

The solution of the boundary value problem by integral transform methods has been reformulated in terms of variables different from those indicated in Reference (9). This has permitted the delineation of the displacement field in terms of quantities derivable from the roots of a sextic algebraic equation whose coefficients depend upon the elastic constants and on the spatial transform parameters. A program has been

written to carry out the necessary numerical computations and test cases are currently under scutiny. Consequently, this aspect of the investigation is approximately three months ahead of schedule. An additional effort will be required to determine an analytical expression for the strain field and to write a program to evaluate this field, so that the results so obtained can be compared directly with strain measurements. This procedure will probably involve a large amount of computational effort, but this appears to be unavoidable since the alternative of numerical differentiation is not a feasible procedure.

A three-dimensional finite element code for a general anisotropic elastic medium has been programmed and found to work effectively in predicting the effects of uniaxial wave propagation in isotropic materials. The results for the three-dimensional case of a point load acting on an isotropic half-space have been found to disagree significantly with those obtained from the corresponding closed-form solution. The indications are that the difficulties encountered can be attributed to the numerical integration scheme employed over the basic finite element. This scheme will be revised and, further, the finite element will be improved. It is expected that upon the resolution of this difficulty, no significant problems will occur when the anisotropic model used in the present investigation is introduced into the program.

The investigations involving the property determinations of the blocks are slightly behind schedule since this phase was initiated almost one-half year subsequent to the beginning of the contract.

However, since many of the techniques to be employed here have previously been utilized extensively in our laboratories, the overall development time for this portion will be considerably less than for the other experimental phases, permitting the expenditure of more time for the gathering of data.

The following section will present in detail the technical accomplishments during the first year of operation of the contract. A subsequent section will discuss the anticipated efforts during the second year of the investigation.

II. TECHNICAL ACCOMPLISHMENTS

The achievements attained during the first year of operation of the contract are described in detail in the following section. The subject matter is subdivided into the following categories: (a) Experimental Examination of the Wave Processes in an Anisotropic Rock Material; (b) Theoretical Examination of the Pulse Propagation Produced in an Anisotropic Solid by a Concentrated Transient Source: (1) Integral Transform Method, and (2) Finite Element Method; and (c) Determination of the Mechanical and Geometrical Properties of the Yule Marble Blocks to be Employed as Half-spaces.

a) Experimental Examination of the Wave Processes in an Anisotropic Rock Material

In the present project, the examination of body and surface waves will be conducted using the two blocks of Yule marble cited previously, with dimensions of $1\frac{1}{2}' \times 1\frac{1}{2}' \times 2'$, one of which was used in the investigation by Ricketts[8][9]. The procedures to be employed also closely parallel this earlier work, but involve significant and innovative extensions.

The specimens will be loaded on the free surface by means of sphere impacts either directly or through an intermediate loading bar; the loading pulse will be monitored by crystals or strain gages at the contact point or on this intermediate bar. The impact will be controlled in order to limit the length of the pulse to a dimension small compared to the size of the block so that observations of the entire initial transmitted pulse at a number of stations can be accomplished without disturbance due to waves reflected from the free surfaces of the specimen.

Such signals from both surface and interior detectors will be photographically recorded using oscilloscopes. Pulse shape variations can be accomplished by the use of spheres of different sizes, other shapes and sizes of strikers, employment of projectiles composed of different materials, or by changing the shape and/or composition of the transmission devices.

The initial effort to produce body-wave sensors utilized 1/8" x 1/32" circular X-cut quartz crystals that measure uniaxial normal stress. The first experiments were performed in rock bars of about 3/4 inch in diameter subjected to central longitudinal impact. This involved the attachment of lead wires to the crystals using Electrobond #2016 adhesive manufactured by Adhesive Engineering Company. A bar about 2 feet long was cut into two by means of a special rock saw and a hole 3/16" in diameter and 3/16" deep was drilled on the centerline of one of the segments. A diametral groove was sliced across the hole to accommodate the lead wires, as shown in Figure 1. The hole was now filled with a mixture of EPY-150 epoxy cement and rock powder, and the crystal was embedded in this composite. The other segment was then bonded to the first to produce a single test specimen with an internal transducer, employing a special alignment jig[8]. A pair of SR-4, FAE-12-12 S9L foil gages were mounted on the opposite ends of a bar diameter at a position about 3 inches from the crystal position by means of EPY-150 cement manufactured by Baldwin-Lima-Hamilton Electronics, Inc., as shown in Figure 2. These gages were incorporated in a potentiometric circuit and were coupled in series to eliminate any antisymmetric components of the transient from the records. A ½"

diameter steel ball was dropped from a height of 4½ feet onto the end face of this bar and the resulting pulse as sensed by both transducers was recorded on an oscilloscope. As shown in Figure 3, certain distortions in the signal were produced by the crystal, but not by the surface strain gage, indicating the need for corrective measures.

In the next experiment, one segment of a similar bar was drilled to a depth of 2" and a diameter of 3/16" as shown in Figure 4 with the sensor attached to the end of the core. The core was then reinserted into the hole in the bar and the remaining void was filled with an epoxy cement; the second segment was attached as before. A similar impact test again inddicated distortion of the crystal signal; this effect was now believed to be due to either a cross effect between longitudinal and lateral strains of the completely embedded crystal or due to inadequate low frequency response of this sensor[11]. The latter is a function of the circuit time constant RC with R and C as the total resistance and capacitance of the circuit, respectively. It had been estimated[11] that if a 3000 μμF capacitance were to be introduced in the circuit by the addition of parallel capacitors, it would permit the reproduction of both peak amplitude and duration of the pulse to within at least 95 percent. However, such a step did not materially improve the signal response. In consequence, this aberration was thus attributed solely to the constraint condition on the embedded crystal.

In view of this conclusion, some attempts were made to isolate lateral crystal surface from the rock walls. This was successfully accomplished by surrounding the crystal with a rubber ring that left

the sides of the sensor essentially unconstrained, as shown in Figure 5, and embedment of this unit within the bar as before. The results of a similar impact test as well as that on the previous crystal arrangement, presented in Figure 6 show that the removal of the lateral constraint on the crystal permits the reproduction of the strain gage signal with much greater fidelity.

These results were compared to those obtained when charge amplification using an Endevco Corporation dual channel charge amplifier with Microdot low noise cables was employed to record the crystal response instead of voltage amplification. A tentative value of 10.0 $\times 10^{-12}$ coulombs/lb was chosen for the piezoelectric constant of the crystal. Figure 7 shows the charge output for the constrained and unconstrained crystal configurations, the latter exhibiting a higher amplitude, obtained from the chopped mode of a single beam oscilloscope trace: these data support the conclusion above concerning the origin of the distortion in the signal. As has been predicted previously[12], the discontinuities due to bonding of the two segments and the transducer embedment had no observable effect on the transmission of the pulse.

Initially, it was deemed necessary to check the consistency of the output from the various crystals obtained from the same source (X-tron Electronics, Inc., Hayward); this was accomplished by performing a split Hopkinson-bar calibration technique[12][13] as shown in Figure 8. X-cut quartz crystals, 1/8" in diameter and 1/32" thick were sandwiched between two 1/8" diameter 2024-T4 aluminum bars, each 15" long, and subjected to longitudinal impact by a 3/16" diameter steel ball fired

from a gun at a low initial velocity. The response from this transducer and from a pair of strain gage stations, each consisting of two sensors at the opposite end of a diameter and connected in series, located just ahead and just behind the crystal were recorded on oscilloscopes that were triggered from the output of a strain gage mounted about 3 inches from the impact end. A Kistler Instrument Corporation Model S/N 477 single channel charge amplifier was used in conjunction with the crystal Excellent correspondence between the rise times and pulse lengths of the two types of records were obtained. The same result was obtained for each of approximately 10 different crystals, indicating in addition to the reproducibility feature that the discontinuity introduced by the crystal yielded no measurable effects.

In order to retain the lateral freedom of the crystal upon insertion in the specimen by preventing the bonding material from surrounding the sensor, and retain its freedom from lateral constraint, it was found to be necessary to mount the crystal inside a housing. Initially, this housing was fabricated from lucite in view of its easy machinability, and the unit was assembled as shown in Figure 9. This was then tested in a 3/16" split aluminum Hopkinson bar similar to the one described above. The signals from the unit showed distinct evidence of reflections caused by impedance mismatch of the lucite relative to the other materials employed. As a consequence, the revised design exhibited in Figure 10 was adopted.

Here, the crystal was encased between two aluminum end pieces separated by a glass washer. The latter was cut with a precision diamond saw to achieve parallel faces from a tube previously etched to

the required dimensions. With this arrangement, the impedance mismatch between the aluminum, quartz and glass components of the unit is minimized. This package was now tested in the split Hopkinson bar arrangement as shown in Figure 11 with good results as portrayed in Figure 12. A total of six crystal packages were assembled and tested in this manner; their response was in excellent agreement with the corresponding strain gage signals. Thus, this technique was also employed for the calibration of the packages.

A piezoelectric crystal is essentially a charge generator and the potential difference V between its faces is given by

$$V = \frac{q}{c_t} \tag{1}$$

where q is the charge generated and c_t is the capacitance of the crystal. If the external capacitance of the circuit is C_s which includes the capacitances of connecting wires, connectors and the input capacitance of the recording device, then

$$V = \frac{q}{c_t + C_s} \tag{2}$$

In the case of the X-cut quartz crystal used in the longitudinal compression mode, the piezoelectric relations reduce to,

$$q = \sigma \cdot A \cdot k \tag{3}$$

where σ is the longitudinal stress, A is the electrode area of the crystal and k is the appropriate piezoelectric constant. Then Eqs. (2) and (3) combine to give

$$\sigma = \frac{V(C_t + C_s)}{AK} = \frac{VC}{AK} \tag{4}$$

In order to establish the values of the circuit constants for the arrangement employed, the capacitances of the crystal, connecting wires, connectors and other external elements were measured by means of an impedance bridge. The total capacitance of the circuit then consisted of these values plus that of the plug-in unit. The circuit resistance consisted essentially only of the oscilloscope input impedance, amounting to 10 megaohms for the type 2A61 plug-in unit used in conjunction with the Tektronix 565 double beam oscilloscope. These data are required in order to compare the piezoelectric constant determined from the output of the transducer package equated to the strain gage signal with published values for this crystal.

The identical split Hopkinson bar technique used in the quality control studies previously cited was employed for the actual calibration. The tests involved the dropping of a $\frac{1}{2}$ inch diameter steel sphere onto the vertical bar arrangement. The strain gages exhibited a gage factor of 2.01, a resistance of 120 ohms, and were calibrated by the dynamic shunting of external resistances into the circuit and observation of the deflection of the trace[14]. This permitted the establishment of the strain-time record and the evaluation of the transducer package response upon comparison of the peak strains, as shown in Figure 12. Values of the corresponding uniaxial stress were obtained by means of a value of 10.6×10^6 psi for the dynamic modulus of the aluminum calibration bars.

With the aid of Eq. (4), the measured total circuit capacitance, the area of the 1/8" diameter crystal face, the peak voltage output and the maximum stress evaluated, the piezoelectric constant was computed

to have an average value of $10.2 \times 10^{-12} \pm 0.2 \times 10^{-12}$ coulombs/lb which compares well with the value of 10.01×10^{-12} coulombs/lb cited by Lion[15]. It was observed that the pulses recorded by the strain geges ahead and behind the crystal were identical. The calibration was performed for three values of external capacitance, i.e. 3,000, 6,000 and 12,000 μμF, and a total of 4 crystal transducers were tested.

After calibration of the transducer packages with a known external capacitance utilized to improve low frequency response, the units were then tested with the aid of a charge amplifier. In this case, the response is independent of the circuit capacitance[14]. The value of the piezoelectric constant k determined from the calibration tests was used to obtain the charge and the stress could then be directly computed. The excellent correspondence between these results is exemplified in Figure 13. All subsequent calibration of the units will utilize the charge amplifier technique in conjunction with the established value of the piezoelectric constant.

An additional physical modification of the transducer unit was required in order to permit ready insertion into relatively long core holes. This was accomplished by a rearrangement of the lead configuration as shown in Figure 14. Although the acoustic impedances of the elements composing the package are nearly identical, they differ significantly from that of the Yule marble specimen in which they are to be inserted. However, in view of the expectation that the length of the pulses generated will be large in comparison with the dimensions of the transducer package, the response is not believed to be significantly affected by this mismatch. Experiments are currently in progress utilizing Yule marble bars to directly verify this hypothesis.

Coring of 3/16" diameter holes in Yule marble bars by means of a diamond drill has shown that the cores could not be recovered due to severe crumbling of the material. Thus, it appeared necessary to first drill a hole, then anchor the transducer package at its base, extract the leads, and then fill and tamp the remaining void with a suitable replacement material. As a preliminary study, several 1-1/16" diameter bars of Yule marble, 9 inches long, were obtained by coring out large slabs of locally available material, and two smooth-faced segments were cut under slow hydraulic feed. A 3/16" diameter hole about 2" long was drilled coaxially in one length of the bar. The crystal transducer was inserted and the hole was filled with a mixture of rock powder and epoxy. A composite bar assembly was made as shown in Figure 15. Strain gages were mounted on the bar at the same section as the crystal station. A dynamic experiment was conducted by dropping a $\frac{1}{2}$" diameter ball on one end of the vertically held assembly. The resulting pulse was recorded by the embedded crystal transducer and the strain gages. Reflections, due to the epoxy rock mixture filler material, occurred which were observed on the oscillograms.

At present further experiments are in progress to select a suitable filler material which would closely match the acoustic impedance of Yule marble. It is thought that this will consist of a mixture of alumina and epoxy in the appropriate proportions, the former having high impedance and the latter having low impedance compared to that of Yule marble. Additional work is also underway to establish a suitable grouting material. However, the development work carried out so far indicates that the installation of the crystal transducer can be accomplished satisfactorily in deep holes.

b) Theoretical Examination of the Pulse Propagation in an Anisotropic Solid Due to a Transient Source

The formulation of the equations governing the boundary value problem of a generally anisotropic half-space subjected to a normal time-dependent point load on the free surface are straightforward. The constitutive relations are

$$\sigma_{ij} = c_{ijk\ell}\, e_{k\ell} = \tfrac{1}{2}\, c_{ijk\ell}\, (u_{k,\ell} + u_{\ell,k}) \tag{5}$$

where u_i is the displacement vector, σ_{ij} and $e_{k\ell}$ are the stress and strain tensors, respectively, and $c_{ijk\ell}$ is the tensor of the elastic constants that satisfy the following symmetry relations

$$c_{ijk\ell} = c_{jik\ell} = c_{ij\ell k} = c_{k\ell ij} \tag{6}$$

In the usual tensor notation, a comma indicates differentiation with respect to the variable (s) following it and the usual summation convention on spatial variables is employed. In a homogeneous medium obeying Eq. (5), for small displacements, the displacement equations of motion under no body forces are given in a rectangular Cartesian coordinate system x_1, x_2, x_3 as

$$c_{ijk\ell}\, u_{k,\ell j} = \rho\, u_{i,tt} \tag{7}$$

where ρ is the mass density and t is time. When the free surface of the half-space is given by $x_2 = 0$, the boundary condition here becomes

$$c_{i2k\ell} u_{k,\ell}(x_1, 0, x_3, t) = -\delta_{i2} f(t)\, \delta(x_1, x_3) \tag{8}$$

where δ_{ij} is the Kronecker delta, f(t) is the arbitrary force history, and $\delta(x_1, x_3)$ is the two-dimensional Dirac delta function; the radiation condition at infinity is also invoked. However, the actual evaluation of the fields for this problem will require extensive numerical

computations which, for the general anisotropic case, may not be feasible at the present time.

In the problem posed above, a transversely anisotropic half-space is considered with the axis of elastic symmetry located in the free surface. The stress-displacement equations for this solid are given by

$$\begin{aligned}
\sigma_{11} &= c_{11}\, u_{1,1} + c_{12}\, u_{2,2} + c_{13}\, u_{3,3} \\
\sigma_{22} &= c_{12}\, u_{1,1} + c_{11}\, u_{2,2} + c_{13}\, u_{3,3} \\
\sigma_{33} &= c_{13}\, (u_{1,1} + u_{2,2}) + c_{33}\, u_{3,3} \\
\sigma_{23} &= c_{44}\, (u_{3,2} + u_{2,3}) \\
\sigma_{13} &= c_{44}\, (u_{3,1} + u_{1,3}) \\
\sigma_{12} &= \tfrac{1}{2}\, (c_{11} - c_{12})\, (u_{1,2} + u_{2,1})
\end{aligned} \tag{9}$$

where the standard contracted notation c_{mn} with m, n = 1,...,6 has been employed instead of the four-index representation c_{ijkl}. The solution of this problem is considerably more tractable and has been attacked by two different procedures: (1) The Integral Transform Technique, and (2) The Finite Element Method. Each of these two methods has unique advantages and disadvantages in the evaluation and interpretation of the results.

The integral transform method utilizing a Laplace-Fourier transform and a Cagniard-de Hoop procedure[6][8][16] is well established and permits interpretation of the wave process in terms of surfaces (velocity, slowness and wave surface) that are associated with phase and group phenomena in the medium. This technique allows the evaluation of any individual response quantity at any point of the medium and at any

specific time without the need for its evaluation at any other space-time point. Thus, the procedure is very efficient if only a few values are desired, but becomes very expensive in terms of machine time if the entire field needs to be evaluated over a prolonged period. The numerical methods required for this analysis lead to errors that are both known and, furthermore, whose size can be controlled readily. On the other hand, this technique also becomes intractable when the phenomena to be investigated involve greater complications of loading, anisotropy, inhomogeneity and boundary conditions. In this respect, the finite element method has distinct advantages, but suffers from the drawbacks of the need for the evaluation of the entire field, the lack of experience in the use of this technique for problems of this kind, and the fact that the discretization procedure is not as well understood or controlled as for the integral transform analysis.

(1) Integral Transform Technique.

The technique to be employed is an adaptation of that utilized by Kraut[6], Ricketts[8] and Burridge[7]. For the transversely isotropic case, Eqs. (7) reduce to

$$\begin{aligned} &c_1 u_{1,11} + c_2 u_{1,22} + c_3 u_{1,33} + (c_1 - c_2)u_{2,21} \\ &\qquad + c_4 u_{3,31} = u_{1,tt} \\ &(c_1 - c_2) u_{1,21} + c_2 u_{2,11} + c_1 u_{2,22} + c_3 u_{2,33} \\ &\qquad + c_4 u_{3,32} = u_{2,tt} \\ &c_4 u_{1,31} + c_4 u_{2,32} + c_3 u_{3,11} + c_3 u_{3,22} + c_5 u_{3;33} = u_{3,tt} \end{aligned} \tag{10}$$

where five new independent constants have been introduced by

$$c_1 = c_{11}/\rho \qquad c_2 = \tfrac{1}{2}(c_{11} - c_{12})/\rho \qquad c_3 = c_{44}/\rho$$
$$c_4 = (c_{13} + c_{44})/\rho \qquad c_5 = c_{33}/\rho \tag{11}$$

The equations of motion and the boundary condition will be subjected to a one-sided Laplace and to a double Fourier transform defined by

$$u_k^*(\vec{x}, s) = \int_0^\infty e^{-st}\, u_k(\vec{x}, t)\, dt \qquad s > 0, \text{ real} \tag{12}$$

and

$$\bar{u}_k^*(\alpha_1, x_2, \alpha_3, s) = \int_{-\infty}^{\infty}\int e^{is(\alpha_1 x_1 + \alpha_3 x_3)}\, u_k^*(\vec{x}, s)\, dx_1\, dx_3 \tag{13}$$

respectively, where $\vec{x}$ is the radius vector from the coordinate origin to a generic point in the medium and $i = \sqrt{-1}$. In transform space, the former become

$$\begin{aligned}
&[c_2D^2 - s^2(c_1\alpha_1^2 + c_3\alpha_3^2 + 1)]\,\bar{u}_1^* - (c_1 - c_2)\,is\alpha_1\,\bar{u}_2^* - c_4\,s^2\alpha_1\alpha_3\,\bar{u}_3^* = 0\\
&-(c_1 - c_2)\,is\alpha_1 D\bar{u}_1^* + [c_1D^2 - s^2(c_2\alpha_1^2 + c_3\alpha_3^2 + 1)]\,\bar{u}_2^* - c_4\,is\alpha_3 D\bar{u}_3^* = 0\\
&-c_4 s^2\alpha_1\alpha_3\,\bar{u}_1^* - c_4\,is\alpha_3\,D\bar{u}_2^* + [c_3D^2 - s^2(c_3\alpha_1^2 + c_5\alpha_3^2 + 1)]\,\bar{u}_3^* = 0
\end{aligned} \tag{14}$$

where the symbol D denotes differentiation with respect to x_2. The corresponding boundary conditions on $x_2 = 0$ are

$$\begin{aligned}
&D\bar{u}_1^* - is\alpha_1\bar{u}_2^* = 0\\
&(c_1 - 2c_2)\,is\alpha_1\bar{u}_1^* - c_1 D\bar{u}_2^* + (c_4 - c_3)\,is\alpha_3\bar{u}_3^* = f^*(s)/\rho\\
&D\bar{u}_3^* - is\alpha_3\bar{u}_2^* = 0
\end{aligned} \tag{15}$$

A solution is now assumed in the form

$$\bar{u}_k^* = U_k\, e^{-s\lambda x_2} \tag{16}$$

which, upon substitution in Eqs. (14), leads to a system of homogeneous algebraic equations in U_k; the condition for a non-trivial solution yields the following determinantal equation

$$\begin{vmatrix} (c_2\lambda^2 - c_1\alpha_1^2 - c_3\alpha_3^2 - 1) & (c_1 - c_2)i\alpha_1\lambda & -c_4\alpha_1\alpha_3 \\ (c_1 - c_2)i\alpha_1\lambda & (c_1\lambda^2 - c_2\alpha_1^2 - c_3\alpha_3^2 - 1) & c_4 i\alpha_3\lambda \\ -c_4\alpha_1\alpha_3 & c_4 i\alpha_3\lambda & (c_3\lambda^2 - c_3\alpha_1^2 - c_5\alpha_3^2 - 1) \end{vmatrix} = 0 \quad (17)$$

Equation (17) is a sextic in λ and defines the slowness surface. For a transversely isotropic material, it degenerates into a quadratic and a quartic factor which greatly simplifies the subsequent analysis.

The slowness surface is given by

$$[(c_1\Lambda^2 - M)(c_3\Lambda^2 - N) + c_4^2\alpha_3^2\Lambda^2](c_2\Lambda^2 - M) = 0 \quad (18)$$

where

$$M = c_3\alpha_3^2 + 1, \qquad N = c_5\alpha_3^2 + 1, \quad \text{and}$$

$$\Lambda^2 = \lambda^2 - \alpha_1^2 .$$

Consequently, the expressions for $\lambda_j = \lambda_j(\alpha_1, \alpha_3)$, with $j = 1, 2, 3$ may be written as

$$\lambda_1 = s_2^{(1)} = [\alpha_1^2 + (c_3\alpha_3^2 + 1)/c_2]^{\frac{1}{2}}$$

$$\lambda_{2,3} = s_2^{(2),(3)} = \left[\alpha_1^2 + \frac{\Phi \pm \sqrt{\Phi^2 - 4c_1c_3MN}}{2c_1c_3}\right]^{\frac{1}{2}} \quad (19)$$

where $\Phi = c_1N + c_3M - c_4^2\alpha_3^2$ and λ_j are to be chosen such that $\mathrm{Re}(\lambda_j) \geq 0$ to satisfy the radiation condition. Substitution of these eigenvalues into the homogeneous algebraic equations yield the three associated eigenvectors $U_k^{(j)}$ so that the general solution to Eq. (14) now takes

the form

$$\bar{u}_k^* = \sum_{j=1}^{3} U_k^{(j)} \, e^{-s\lambda_j x_2} \tag{20}$$

If the three independent $U_k^{(j)}$ are chosen as $U_1^{(j)}$, then Eq. (20) may be written as

$$\begin{aligned}
\bar{u}_1^* &= U_1^{(1)} \, e^{-s\lambda_1 x_2} + U_1^{(2)} \, e^{-s\lambda_2 x_2} + U_1^{(3)} \, e^{-s\lambda_3 x_2} \\
\bar{u}_2^* &= -(i\alpha_1/\lambda_1) \, U_1^{(1)} \, e^{-s\lambda_1 x_2} - (i\lambda_2/\alpha_1) \, U_1^{(2)} e^{-s\lambda_2 x_2} \\
&\qquad - (i\lambda_3/\alpha_1) \, U_1^{(3)} \, e^{-s\lambda_3 x_2} \\
\bar{u}_3^* &= \frac{1}{\alpha_1 \alpha_3} \left[b_2 \, U_1^{(2)} \, e^{-s\lambda_2 x_2} + b_3 \, U_1^{(3)} \, e^{-s\lambda_3 x_2} \right]
\end{aligned} \tag{21}$$

where $b_j = (c_1 \lambda_j^2 - M)/c_4 \; ; \quad j = 2,3.$

The general solution, Eq. (21), is then adjusted to satisfy the boundary conditions, Eqs. (15), yielding three equations in $U_1^{(j)}$

$$\begin{aligned}
&(\lambda_1^2 + \alpha_1^2) U_1^{(1)} + 2\lambda_1 \lambda_2 \, U_1^{(2)} + 2\lambda_1 \lambda_3 \, U_1^{(3)} = 0 \\
&L_1 U_1^{(1)} + L_2 U_1^{(2)} + L_3 U_1^{(3)} = i\alpha_1 f^*(s)/\rho s \\
&\alpha_1^2 \alpha_3^2 \, U_1^{(1)} + \lambda_1 \lambda_2 (\alpha_3^2 + b_2) U_1^{(2)} + \lambda_1 \lambda_3 (\alpha_3^2 + b_3) U_1^{(3)} = 0
\end{aligned} \tag{22}$$

where $L_1 = 2c_2 \alpha_1^2,$

$$L_K = L_1 + c_1 \Lambda_K^2 - (c_4 - c_3) b_k \; , \; k = 2, 3.$$

The relations are now solved for the $U_1^{(j)}$, and substitution of these values into Eq. (21) yields the displacement field in transform space

$$\vec{u_1^*} = f^*(s)\,\frac{i\alpha_1}{\varphi s D_0}\left[A_1\, e^{-s\lambda_1 x_2} + A_2\, e^{-s\lambda_2 x_2} + A_3\, e^{-s\lambda_3 x_2}\right]$$

$$\vec{u_2^*} = f^*(s)\,\frac{1}{\rho s D_0}\left[\frac{\alpha_1^2}{\lambda_1} A_1 e^{-s\lambda_1 x_2} + \lambda_2 A_2\, e^{-s\lambda_2 x_2} + \lambda_3 A_3\, e^{-s\lambda_3 x_2}\right] \qquad (23)$$

$$\vec{u_3^*} = f^*(s)\,\frac{1}{\rho s \alpha_3 D_0}\left[b_2 A_2\, e^{-s\lambda_2 x_2} + b_3 A_3\, e^{-s\lambda_3 x_2}\right]$$

where $D_0 = A_1 L_1 + A_2 L_2 + A_3 L_3$

$$A_1 = -\,2\lambda_1\lambda_2\lambda_3\,(b_3 - b_2)$$

$$A_2 = \lambda_3[\Lambda_1^2(\alpha_3^2 + b_3) + 2\alpha_1^2\, b_3]$$

$$A_3 = -\,\lambda_2[\Lambda_1^2(\alpha_3^2 + b_2) + 2\alpha_1^2\, b_2]\,.$$

Using the Fourier inversion theorem yields the solution in the Laplace transform space as

$$u_k^*(\vec{x},s) = \frac{s f^*(s)}{4\pi^2 \rho}\int_{-\infty}^{\infty}\int \sum_{j=1}^{3} W_k^{(j)}(\alpha_1,\alpha_3)\, e^{-s(i\alpha_1 x_1 + i\alpha_3 x_3 + \lambda_j x_2)}\, d\alpha_1 d\alpha_3 \qquad (24)$$

where

$$W_1^{(j)} = \frac{i\alpha_1}{D_0} A_j \quad , \; j = 1,\ 2,\ 3$$

$$W_2^{(1)} = \frac{\alpha_1^2}{\lambda_1 D_0} A_1 \quad , \quad W_2^{(j)} = \frac{\lambda_j}{D_0} A_j \quad , \; j = 2,\ 3$$

$$W_3^{(1)} = 0 \qquad , \quad W_3^{(j)} = \frac{i b_j}{\alpha_3 D_0} A_j \quad j = 2,\ 3$$

The inversion of Eq. (24) into the real time domain is expedited by the transform

$$\alpha_1 = w\cos\theta = -\,ip\cos\theta$$

$$\alpha_3 = w\sin\theta = -\,ip\sin\theta \qquad -\infty < w < \infty\ ;\ -\tfrac{1}{2}\pi \le \theta < \tfrac{1}{2}\pi \qquad (25)$$

where the Jacobian of the transformation is $|J(p, \theta)| = p$ and p is considered to be complex. Furthermore, a polar coordinate system in the x_1x_3-plane is introduced, given by

$$x_1 = r\cos\tilde{\theta} \qquad x_3 = r\sin\tilde{\theta} \quad \text{with } 0 \le r < \infty \text{ and } 0 \le \tilde{\theta} < 2\pi \tag{26}$$

Equation (24) is now rewritten as

$$u_k^*(\vec{x},s) = -\frac{1}{4\pi^2\rho}\int_{-\frac{\pi}{2}}^{\frac{\pi}{2}} d\theta \int_{-i\infty}^{i\infty} sf^*(s)\sum_{j=1}^{3} W_k^{(j)}(p,\theta)p\, e^{-s[pr\cos(\tilde{\theta}-\theta)+\lambda_j x_2]}\, dp \tag{27}$$

It is inverted utilizing the Cagniard-de Hoop method[16] in which new variables are introduced by means of the relations

$$\begin{aligned} \mathrm{Re}[pr\cos(\tilde{\theta}-\theta) + \lambda_j(p,\theta)\, x_2] &= t_j\ , \\ \mathrm{Im}[pr\cos(\tilde{\theta}-\theta) + \lambda_j(p,\theta)\, x_2] &= 0 \end{aligned} \tag{28}$$

where t_j is real and positive. These relations define three sets of parametric relations in t_j for the Cagniard-de Hoop path on the complex p-plane. Using Cauchy's integral theorem and Jordan's Lemma, it can be shown that integration along the Bromwich contour for Eq. (27) is equivalent to integration along the Cagniard-de Hoop path[6].

Equation (28) may be expressed as a polynomial p as

$$\begin{aligned} &p^2\{\cos^2\varphi\,\cos^2(\tilde{\theta}-\theta) + (\cos^2\theta + \frac{c_3}{c_2}\sin^2\theta)\sin^2\varphi\} \\ &- p[2\tau\cos\varphi\cos(\tilde{\theta}-\theta)] + [\tau^2 - \frac{\sin^2\varphi}{c_2}] = 0 \end{aligned} \tag{29}$$

and

$$p^4 + A(\tau,\tilde{\theta},\tilde{\theta},\varphi)p^3 + B(\tau,\tilde{\theta},\theta,\varphi)p^2 + C(\tau,\tilde{\theta},\theta,\varphi)p + E(\tau,\tilde{\theta},\theta,\varphi) = 0 \tag{30}$$

for the quadratic factor involving λ_1 and the quartic factor involving λ_2 and λ_3, respectively, in Eq. (19)

where, $\tau = t/R$,

$$A = -\frac{2}{F}\left(2\tau \cos^3\varphi \cos^3(\tilde{\theta}-\theta) + \tau G \cos\varphi \cos(\tilde{\theta}-\theta) \sin^2\varphi\right],$$

$$B = \frac{1}{F}\left[6\tau^2 \cos^2\varphi \cos^2(\tilde{\theta}-\theta) + \tau^2 G \sin^2\varphi - \sin^2\varphi \cos^2\varphi \cdot \cos^2(\tilde{\theta}-\theta)\, e_1 - \sin^4\varphi\, J\right]$$

$$C = -\frac{2}{F}\left[2\tau^3 \cos\varphi \cos(\tilde{\theta}-\theta) - \tau \cos\varphi \sin^2\varphi \cos(\tilde{\theta}\ \theta) e_1\right]$$

$$E = \frac{1}{F}\left[\tau^4 - \tau^2 \sin^2\varphi\, e_1 + \sin^4\varphi\, h_1\right]$$

$$F = \cos^4\varphi \cos^4(\tilde{\theta}-\theta) + \sin^2\varphi \cos^2\varphi \cos^2(\tilde{\theta}-\theta) G + \sin^4\varphi\, K$$

$$K = \cos^4\theta + (2-m_1) \sin^2\theta \cos^2\theta + \frac{c_5}{c_1} \sin^4\theta$$

$$J = e_1 \cos^2\theta + f_1 \sin^2\theta ,$$

$$G = 2 - m_1 \sin^2\theta$$

$$m_1 = h_1(2c_1c_3 - c_1c_5 - c_3^2 + c_4^2)$$

$$e_1 = h_1(c_1 + c_3)$$

$$f_1 = h_1(c_3 + c_5)$$

$$g_1 = h_1(c_1 - c_5)$$

$$h_1 = 1/c_1c_3$$

In the above, an additional space transformation is introduced, given by

$$R = (r^2 + x_2^2)^{\frac{1}{2}} , \quad 0 \le R < \infty ; \quad \varphi = \tan^{-1}\frac{x_2}{r} , \quad 0 \le \varphi < \pi \qquad (31)$$

Since Eqs. (29) and (30) are polynomials in powers of p with real coefficients, their roots are either real or complex conjugate. Upon deforming the path of integration of Eq. (27) into Cagniard-de Hoop contours, recalling that s and τ are real and taking advantage of the

symmetry of the path with respect to the real axis of the p plane, there results

$$u_k^*(\vec{x},s) = \frac{-1}{2\pi^2 \rho R} \int_{-\frac{\pi}{2}}^{\frac{\pi}{2}} d\theta \int_{t_j}^{\infty} sf^*(s) \sum_{j=1}^{3} [\mathrm{Re}\ W_k^{(j)}(p,\theta,\tilde{\theta},\varphi)]p \frac{\partial p}{\partial t} e^{-st_j}\, dt \qquad (32)$$

The inversion of this relation into the real time domain is now obtained by inspection as

$$u_k(\vec{x},t) = \frac{-1}{2\pi^2 \rho R} \int_{-\frac{\pi}{2}}^{\frac{\pi}{2}} d\theta \int_{t_j}^{t} \dot{f}(t-t') \sum_{j=1}^{3} \mathrm{Re}[W_k^{(j)}(p,\theta,\tilde{\theta},\varphi)] \; p(t') \frac{\partial p(t')}{\partial t} H(t-t_j)\, dt' \qquad (33)$$

To effect this procedure with any degree of facility, it was necessary to define Riemann surfaces for the Cagniard-de Hoop paths defined by Eqs. (29) and (30) where the values of p are single-valued and analytic. Since there are three branches of λ_j derived from the sextic equation (19), there must exist three such Riemann sheets. If such surfaces are not utilized in the inversion process, then p will be a multi-valued function and the analysis becomes vastly more complicated and tedious[6].

The time function f(t) will now be replaced in Eq. (33) by the Dirac delta function $\delta(t)$, and the Heaviside function $H(t) = \begin{matrix} t \geq 0 \\ t < 0 \end{matrix}$, respectively, yielding

$$u_{k_\delta}(\vec{x},t) = -\frac{1}{2\pi^2 \rho R} \int_{-\frac{\pi}{2}}^{\frac{\pi}{2}} d\theta \left[\frac{\partial}{\partial t}\left\{\sum_{j=1}^{3} \mathrm{Re}\left[W_k^{(j)}(p,\theta,\tilde{\theta},\varphi)\right]\right\} p \frac{\partial p}{\partial t} H(t-t_j)\right] \qquad (34)$$

$$u_{k_H}(\vec{x},t) = -\frac{1}{2\pi^2\rho R}\int_{-\frac{\pi}{2}}^{\frac{\pi}{2}} d\theta\left[\sum_{j=1}^{3} Re[w_k^{(j)}(p,\theta,\tilde{\theta},\varphi)]\; p\;\frac{\partial p}{\partial t}\; H(t-t_j)\right] \qquad (35)$$

Equation (34) is the Green's function for the present dynamic problem and the displacement field for an arbitrary time-dependent force f(t) may be obtained by convolution of this function with f(t). Equation (35) represents another relation that may be employed to obtain a general solution for an arbitrary time history upon convolution with $\frac{d}{dt}$ f(t). The latter is a more convenient relation for this purpose since the kernel function need not be differentiated with respect to time.

It should be noted that, although $\tilde{\theta}$ and θ are independent variables in two separate spaces, the integrands of Eqs. (33) to (35) are related to the response on the $\tilde{\theta}$ = constant plane due to a corresponding line source at $\tilde{\theta} = \theta \pm 90°$ in the two-dimensional solution[6] due to the principle of duality between the slowness space, where θ is defined, and the wave surface[17]. Consequently, the solutions of these equations can also be considered as the superposition of the responses of a continuous distribution of line sources in all directions within the $x_2 = 0$ plane upon multiplication by a weighting factor.

For the propagation of surface waves, the Cagniard-de Hoop path collapses to the real axis of p which contains the Rayleigh pole. Since the path of integration must be deformed to exclude this singularity, the resulting infinitesimal semicircle no longer corresponds to real time and the contribution from the Rayleigh pole must be evaluated separately. This contribution is given by

$$u_{k_{pole}}(x_1, 0, x_3, t) = B_1 \cdot \delta\left(t - \frac{r}{v_R(\tilde{\theta},\theta)}\right) \tag{36}$$

where $v_R(\tilde{\theta},\theta)$ is the Rayleigh wave velocity obtained from the location of the pole and constant B_1 is given by

$$B_1 = Re \left| \frac{i}{\pi\rho} \int_{-\frac{\pi}{2}}^{\frac{\pi}{2}} Q(\tilde{\theta}, \theta, p)\, d\theta \right| \tag{3.}$$

with Q as the residue of the expression

$$\sum_{j=1}^{3} Re \left| w_k^{(j)}(p, \theta, \tilde{\theta}) \right| \tag{38}$$

appearing in Eqs. (34) and (35) at the Rayleigh pole.

Except for the determination of the stress field, the equations presented above conclude the formal analysis of the problem and the evaluation of the field variables requires the use of appropriate numerical methods as detailed below. It is expedient as an intermediate step to compute certain physical features closely associated with the analysis, i.e. the slowness and wave curves and the Cagniard-de Hoop paths for the body waves.

The slowness curves are evaluated by fixing either θ or φ in Eq. (17). Figure 16 shows a set of three slowness curves for a value of $\theta = 90°$ with φ varying from 1° to 89° in increments of 2°, with the s_1 and s_3 axes corresponding to the inverse of the phase velocities along the x_1 and x_3 axes of the medium. The dynamic elastic constants employed in this analysis are those utilized by Ricketts[8] as shown in Table 1.

TABLE 1. VALUES OF DYNAMIC ELASTIC CONSTANTS FOR A YULE MARBLE BLOCK[8].

$$c_1 = 3.8 \times 10^{10} \text{ in}^2/\text{sec}^2$$

$$c_2 = 1.28 \times 10^{10} \text{ in}^2/\text{sec}^2$$

$$c_3 = 0.745 \times 10^{10} \text{ in}^2/\text{sec}^2$$

$$c_4 = 1.89 \times 10^{10} \text{ in}^2/\text{sec}^2$$

$$c_5 = 3.33 \times 10^{10} \text{ in}^2/\text{sec}^2$$

Such curves have already been reported in Reference (8) for both body and surface waves.

Wave curves can also be obtained by fixing either θ or Ψ and are usually evaluated by the rather complicated procedure of taking polar reciprocals of the slowness surface. In the present analysis, they will be determined by a simpler procedure. By virtue of Eq. (28), the Cagniard-de Hoop transformation may be considered as the equation of a plane in the slowness space which is normal to the position vector of a receiver station. With increasing time, this plane moves outward from the origin while maintaining its normality with the position vector. At some particular time t_1, this plane will become tangent to a slowness surface and it can be then considered as a point on the wave surface from the principle of duality. Thus the wave surface can be regarded as being composed of the totality of such tangent planes, each associated with a different radius vector.

Furthermore, these tangent points correspond to the double roots of the Cagniard-de Hoop paths defined by Eqs. (29) and (30). Thus the

discriminants D_p associated with the solutions for p of these equations must vanish and the roots are real since the coefficients in the equations are real. Consequently, the first of these conditions permits the evaluation of the quantity τ, the arrival time at a given receiver station, from a relation of the form

$$D_p(\tau, \tilde{\theta}, \theta, \varphi) = 0 \tag{39}$$

By introducing the variable $\tau = 1/v$ in Eq. (39) and solving this equation for various values of p, each corresponding to a value $v_i(\tilde{\theta}, \theta, \varphi)$, a plot of

$$R_i = v_i(\tilde{\theta}, \theta, \varphi) \cdot t \qquad \text{at } t = 1 \tag{40}$$

provides the wave surface. Figures 17 and 18 show the pair of wave curves on the plane $\tilde{\theta} = 90$ for φ varying from 1° to 90° and on the plane $\varphi = 45°$ for various values of $\tilde{\theta}$, which are obtained from the $D_p(\tau, \tilde{\theta}, \theta, \varphi) = 0$ of Eq. (30), respectively. The first of these diagrams indicates that there exist three characteristic ranges for this medium, $0 \leq \varphi_a < \varphi_1$, $\varphi_1 < \varphi_b < \varphi_2$ and $\varphi_2 < \varphi_c < 90°$, while the second portrays two ranges for $\tilde{\theta}$, namely $0 < \tilde{\theta}_a < \tilde{\theta}_1$ and $\tilde{\theta}_1 < \tilde{\theta}_b < 90°$. The cusps in these curves represent characteristics not exhibited by an isotropic medium. Thus the normal number of roots of Eq. (39) is three, but in the critical angular ranges φ_b and $\tilde{\theta}_b$, there are four such roots for a transversely isotropic material.

A computer program was developed which solves the quartic equation (30) denoting the Cagniard-de Hoop path, employing Bairstow's method[18], and the results are indicated in Figures 19, 20, and 21. The curves clearly indicate the nature of the critical regions of the wave surfaces

as discussed above, with only Figure 20 showing four intersections of the path with the real axis. Sheets I, II, and III of the path correspond to values of λ_1, λ_2 and λ_3, respectively, each converging to an asymptote for large values of τ. A number of other Cagniard-de Hoop paths and slowness and wave curves have been evaluated, but are not reproduced here since they do not exhibit any additional unusual features.

A computer program has also been written to evaluate the displacement field from Eq. (35); this is currently in the process of debugging. It may be necessary to revise and improve the program in order to reduce the required computer time for the location of the real and complex roots of the Cagniard-de Hoop path, a process that appears to be more costly than necessary. The program also determines the real roots for Eq. (39) by equating the discriminant to zero and entails a polynomial evaluator and an integration scheme employing Simpson's rule. Presently, a period of two seconds is required to compute the displacement field at a specified point and a given instant of time. The total computer time for the evaluation of a displacement field along a given ray of the domain resulting from a Heaviside input is a linear function of the number of time intervals that are to be included in history of the transient. It should be noted that, for a given ray, the displacements are calcuated for given values of τ R, and thus the history at all points along such a line can be scaled in accordance with this parameter. For fifty time intervals, approximately one-half hour of computer time on the CDC 6600 would be required to evaluate the displacements along 50 rays. In addition, a convolution integral

procedure must be programmed in order to accommodate specified input histories; such a process is estimated not to be very time-consuming.

Figure 22 presents preliminary results for the Cartesian displacement components u_1, u_2, $u_3(\vec{x}, t)$ for $\theta = 80°$ and $\varphi = 45°$ for a sequence of 19 time intervals, beginning with a spacing of 0.1×10^{-5} sec/in from $\tau = 0.4 \times 10^{-5}$ to 0.8×10^{-5} sec/in and an interval of 0.2×10^{-5} sec/in beyond this range. The time of computation was about 37 seconds; the angle $\varphi = 45°$ was chosen since it lies in the critical range. This diagram exhibits drastically different characteristics than for the corresponding two-dimensional solution[6], primarily in the absence of strong discontinuities that are present in the two-dimensional case. Displacements in cylindrical and spherical components have also been computed for subsequent comparison, but are not included in the present report.

(2) Finite Element Method.

A finite element computer code, FEAP-71 developed by Professor R. L. Taylor of the Department of Civil Engineering, University of California, Berkeley, is being adapted for use on the subject problem. It is a research oriented finite element assembly program with a current selection library of twenty elements and extensive input-output utility routines and automatic error checking. Extensions developed here consist of the construction of a three-dimensional element and associated time integration schemes suitable for use in a wave propagation problem.

The dynamic formulation of the finite element method can be derived from Lagrange's Central Principle which combines virtual work and D'Alembert's Principle. The virtual work statement in a continuous body

can be expressed in indicial notation as

$$\int_V \rho \ddot{u}_i \, \delta u_i \, dV + \tfrac{1}{2} \int_V \sigma_{ij} \, \delta e_{ij} \, dV = \int_S T_i \, \delta u_i \, dS + \int_V F_i \, \delta u_i \, dV \tag{41}$$

where δ is the variation, and T_i, F_i V and S are the components of the surface traction and body force, and the volume and surface of the body, respectively. In order to obtain the displacement equations of motion, the stress and strain terms in Eq. (41) are converted by means of the constitutive equation and the strain-displacement relations; the surface integral is transformed into a volume integral by means of the divergence theorem. The finite element approximation is now introduced by subdividing the domain V and introducing a local Ritz technique such that for each element, the displacements are approximated by

$$u_i(\vec{x}, t) = \langle \varphi_i(\vec{x}) \rangle \{\hat{u}(t)\} \tag{42}$$

where $\langle \varphi_i(\vec{x}) \rangle$ is the row vector of prescribed interpolation functions and $\{\hat{u}(t)\}$ are the nodal displacements represented by a column vector of generalized coordinates. Insertion of Eq. (42) into the displacement version of the virtual work statement yields the set of coupled linear differential equations

$$[M] \{\ddot{\hat{u}}\} + [K] \{\hat{u}\} = \{f\} \tag{43}$$

where [M] is the diagonal mass matrix, [K] is the global stiffness matrix, $\{\hat{u}\}$ is the nodal displacement vector for the entire domain, $\{\ddot{\hat{u}}\}$ is the nodal acceleration vector, and $\{f\}$ is the loading vector.

The solution of Eq. (43) is accomplished by using Newmark's Beta Method[19] which is a step-by-step forward integration procedure, given by

$$\dot{u}_{n+1} = \dot{u}_n + (1 - \gamma)\,\ddot{u}_n \Delta t + \gamma \ddot{u}_{n+1} \Delta t \tag{44}$$

$$u_{n+1} = u_n + \dot{u}_n \Delta t + (\tfrac{1}{2} - \beta)\ddot{u}_n (\Delta t)^2 + \beta \ddot{u}_{n+1} (\Delta t)^2 \tag{45}$$

where β is a parameter characterizing acceleration over the interval Δt, γ is a quantity that introduces artificial damping, Δt is the time step increment and u_n, $\dot{u}_n$ and $\ddot{u}_n$ are the displacements, velocities and accelerations at time step n, respectively.

Upon inspection of Eqs. (43) - (45), it is clear that the solution algorithm is implicit in that the displacement at time $t + \Delta t$ is dependent upon the acceleration at this time, thus requiring either a costly direct solution or an iterative procedure. However, if the Newmark parameter β is chosen as zero, an explicit algorithm results so that the displacement at the new time can be obtained from information available at the previous instant. Such a choice requires the exercise of considerable care to insure that the numerical procedure is stable. Experience has shown that stability can be achieved by appropriate selection of the time step, namely that the time step be less than the ratio of the minimum inter-node distance to the maximum wave speed. This approach was selected here to substantially reduce computer time.

The majority of the effort in this phase thus far has been the coupling of the Newmark explicit method with the original finite element code, FEAP-71. In addition, several programming tricks have been incorporated which greatly reduce computer storage and time requirements. The half-space is modelled by a mesh of identical elements that requires the formation of only a single element stiffness. Moreover,

the formation of the global stiffness matrix [K] which requires massive storage on slow speed devices has been abandoned. Instead, the operations involving this matrix from Eq. (43) are performed by manipulating single element stiffness.

After assembly of this program, initial efforts were concentrated on the debugging phase in which a simple test problem was devised that consisted of the axial loading by a triangular pulse of a stack of cubic elements with eight nodes per element, termed Brick-8. This three-dimensional model collapses to the uni-axial homogeneous elastic wave propagation problem when the medium is treated as a homogeneous, isotropic elastic substance with a Poisson ratio of zero. The results of this check are presented in Figure 23 which shows the excellent correspondence of the predictions of the finite element method and that of classical analysis.

The confidence gained by this agreement prompted the construction of a more complicated test problem, close in character to the case under consideration in this study, for which closed-form analytical solutions as well as other numerical data were available. This consisted of the determination of the response of the isotropic elastic half-space under concentrated time-dependent normal load, as shown in Figure 24a, with the three-dimensional finite element model shown in Figure 24b. Here, the most difficult aspects of the entire procedure, namely the choice of a suitable element including higher-order interpolation functions, the time step and the spatial discretization were to be examined initially. The region in which it is most difficult to obtain accurate results by the finite element method is the domain close to the

concentrated load and on the surface of the half-space where discontinuities associated with the Rayleigh wave dominate. If suitable correlation of the finite element computations with closed-form solutions are obtained in this region, then even better agreement is expected to exist in the remainder of the space.

In view of the fact that extensive testing of the efficacy of the element and optimality of the spatial discretization on a three-dimensional basis is extremely expensive, this aspect of the numerical investigation was performed initially using an axisymmetric (i.e. two-dimensional) finite-element formulation as indicated in Figure 24c. This code is adequate to ascertain the validity of the choices involving these two items, but it cannot be employed in the analysis of the actual problem since the anisotropy encountered here destroys the axisymmetric nature of the phenomenon. Thus, upon completion of this phase of the numerical investigation, the three-dimensional code will be tested directly with particular emphasis on the aspects relating to the anisotropic nature of the problem.

The initial results involving a comparison of the finite-element method and a numerical convolution with a closed-form solution of this problem[20] for a pulse of the form $f(t) = (\sin 2\pi t)^2$ for $0 \leq t \leq 0.5$ and zero otherwise applied at the coordinate origin to the surface of an isotropic half-space with a Young's modulus $E = 2.5$, a Poisson ratio $\nu = \frac{1}{4}$ and a density $\rho = 1$ are presented in Figures 25a, 25b, and 25c. The shape of the pulse corresponds to that observed experimentally at the impact point when a steel sphere is dropped on a block of rock[8]. The diagrams exhibit the vertical surface displacements at three

positions near the impact point as a function of time for both the three-dimensional and the axi-symmetric finite element analysis, as well as the results derived from the closed-form solution. It may be observed that, although the correspondence between the three sets of data nearest the contact point is not outstanding, it dramatically improves, as expected, with distance from the impact point as would also be anticipated to occur in the interior of the medium. In particular, there is close correspondence between the two- and three-dimensional finite element results at points x = 0.2 and 0.3 inches, indicating the validity of the previous conclusion that extensive testing of the efficacy of the code can be performed with the simpler model. As further modifications of the program are initiated, it is expected that the concurrence between the data presented here will improve.

c) Property Determination of Yule Marble

The overall objective of this phase of the investigation consists of the determination of the geometric and mechanical properties of Yule marble, including fracture properties, as a function of strain rate. The material is considered to be transversely isotropic based on both previously published information concerning this rock and the nature of its geologic formation, and its crystal size is such that it can be considered as macroscopically homogeneous in relation to the wave lengths of transients produced in presently available experimental specimens. Five major subdivisions of the testing program can be differentiated: (1) The determination of the axis of transverse isotropy of the material, principally by use of crystallographic

techniques, (2) the execution of quasi-static tests on specimens whose axes are parallel or perpendicular to the axis of transverse isotropy to provide stress-strain curves in tension and compression, at rates ranging from 10^{-5} to 10^{-1} per second, as can be obtained in standard testing machines, (3) the development of procedures to obtain intermediate strain rates of the order of 10 to 100 per second by modifying the split Hopkinson-bar technique, (4) the specification of the variation of the behavior of the material in tension and compression as a function of strain rate, and (5) the characterization of the failure process in terms of the strain-rate parameter, including optical observations of the phenomenon. From this information, a comprehensive model of the mechanical response of the substance may be evolved.

The determination of the axis of transverse isotropy is accomplished crystallographically by microscopic examination of thin sections obtained from three mutually orthogonal directions. These are prepared by first cutting the rock into thin slabs, attaching these slices to glass slides with Canada balsam, and then lapping the rock with fine abrasive until the desired thickness is obtained. Since marble is a matrix of calcite crystals with optical axes oriented randomly about a general preferred direction, it is possible to determine each particular crystal orientation by measuring the angle between the optic axis of a given crystal and some fixed reference[21] direction and plotting this relationship on an equal area projection. When a large number of crystal axes are located, a general pattern of average crystal orientation emerges.

These measurements are performed by locating a uniaxial interference figure, a metalope[21], produced by light passing along the optic axis of a calcite crystal. Each crystal is observed under a microscope equipped with a universal stage which permits the specimen to be rotated about two independent axes corresponding to Euler angles so that the optic axis can be aligned to produce a metalope centered on the crosshair.

While X-ray techniques provide another way of establishing the orientation of the axis of transverse isotropy, this method is elaborate, time-consuming and expensive including the necessity of some computer programming. In consequence, it is not anticipated that this procedure will require employment in the present investigation.

In order to retain the integrity of the two large marble blocks intended for wave propagation studies, slabs with dimensions of 1' X $2\frac{1}{2}$' X $1\frac{1}{4}$" were purchased from Clervi Marble Company, San Francisco for the purpose of furnishing specimens for static testing. Since the axis of transverse isotropy for this slab was unknown, cylindrical test samples 3/4" in diameter X 2" long were simply cored from this source in three mutually orthogonal, albeit arbitrary directions and lapped to within 5/10,000th of parallel. In order to prevent crumbling or splitting out during the coring process, a glass plate was cemented with Canada balsam to the distal side of the slab.

The state of strain in these specimens were measured by means of SR-4 foil resistance gages mounted by means of Epoxy 150 cement. A compromise was required to select a suitable size for this transducer. A gage of excessive size records the average strain across a region, not

at a point, and, further, is more difficult to attach; a gage too small covers too few crystals to represent the behavior of the material on a macroscopic scale. The optimum size was ascertained to be a ½" gage length, and the gage employed was a Baldwin-Lima Hamilton paper-backed SR-4 type FAP transducer with a resistance of 120 ohms and a gage factor of 2.01. These gages were attached on opposite ends of a diameter and coupled in series to eliminate any bending components present. The gages were incorporated in an AC-excited bridge circuit including an amplifier and the output was recorded on a plotter. The records were calibrated by means of the insertion of ten known shunt resistances across the gage. The applied compressive force was determined by means of a calibrated cell with a 0 - 10,000 lb range that concurrently recorded the ordinate of the stress-strain curve.

In order to measure the presence of bending which should be minimized or preferably eliminated from these static tests, the two longitudinal gages were decoupled and read individually. Initial use of various types of end pieces including a ball and socket, rubber sheets and plaster capping yielded deviations as high as 50 percent. The best results were obtained with the aid of the capping material Hydrostone which consists of a modified Plaster of Paris base. This material was mixed with water and allowed to set on the specimen at a pressure of 20 psi for 45 minutes. This reduced the deviation between the gage readings to the 10-15 percent range; some of this is unavoidable due to local inhomogeneities and the nonrandom orientation of crystals under each gage.

A typical compressive quasi-static stress-strain curve is presented in Figure 26, clearly exhibiting the nonlinear response of the material. Figure 27 shows the first and the tenth strain cycle when a specimen was repeatedly and continuously loaded to 750 lb and then unloaded, all at the same strain rate. Both curves indicate the presence of hysteresis, but the repeated loading apparently diminishes this effect while increasing the apparent stiffness. Further tests along this line under varying strain rates are in progress.

The development of tests to produce intermediate strain rates consisted of two approaches, the first of which attempted to transform a long rectangular loading pulse produced by the impact of a long cylinder on a Hopkinson bar into a triangular pulse which exhibits a predetermined constant strain rate. This concept employs the idea of a mechanical converter which exploits the impedance mismatch of concentric bars of various radii and material properties as shown in Figure 27 to transform such a rectangular input pulse as shown in Figure 28. The transmission and reflection coefficients, T and R, respectively, for this converter are given by[12]

$$T_{12} = \left[\frac{2A_1\rho_2c_{0_1}}{A_1\rho_1c_{0_1} + A_2\rho_2c_{0_2}}\right] \qquad R_{121} = \left[\frac{A_2\rho_2c_{0_2} - A_1\rho_1c_{0_1}}{A_1\rho_1c_{0_1} + A_2\rho_2c_{0_2}}\right]$$

$$T_{23} = \left[\frac{2A_2\rho_3c_{0_3}}{A_2\rho_2c_{0_1} + A_3\rho_3c_{0_3}}\right] \qquad R_{232} = \left[\frac{A_3\rho_3c_{0_3} - A_2\rho_2c_{0_2}}{A_2\rho_2c_{0_2} + A_3\rho_3c_{0_3}}\right] \qquad (46)$$

$$T_{21} = \left[\frac{2A_2\rho_1c_{0_1}}{A_1\rho_1c_{0_1} + A_2\rho_2c_{0_1}}\right] \qquad R_{212} = \left[\frac{A_1\rho_1c_{0_1} - A_2\rho_2c_{0_2}}{A_1\rho_1c_{0_1} + A_2\rho_2c_{0_2}}\right]$$

where A and c_0 are the cross-sectional area and the rod wave velocity of the various elements, respectively. The output of this converter to an input history f(t) is given by

$$R(t) = T_{12}T_{23} \sum_{n=0}^{\infty} (R_{212}R_{232})^n f\left(t - n\left[\frac{2\ell}{c_{0_2}}\right]\right) \tag{47}$$

For a rectangular input waveform of unit amplitude and duration T^*, choosing ℓ to be such that $c_{0_2} = 10\ell/T^*$, and with $(R_{212}R_{232}) = 0.8$, $T_{12}T_{23} = 0.035$, the pulse is converted into an approximately triangular shape as shown in Figure 29. Other input histories would be deformed in an analogous fashion.

One of the difficulties associated with this process is evident by inspection of Figure 29, namely the high signal loss through the converter. It may also be noted that the output is not truly ramp-shaped, but rather multistepped with an average slope which decays with time.

The second method of obtaining intermediate strain rates considered is the impact of a long cylinder prefaced by a cone on a Hopkinson bar. Numerous materials and cone geometries of the composite striker were tested, the most successful results being obtained with a 30° steel cone mounted on the end of a $\frac{1}{2}$" diameter, 8" long 7075 aluminum bar. Strain rates of 10 sec^{-1}, linear over the entire range of strains were obtained in a 7075 aluminum Hopkinson bar, as shown in Figure 30a. In a standard Hopkinson bar test, the strain rates are of the order of 1000 sec^{-1}. With the present device, the rate can be reduced from this value only to a level of about 50 sec^{-1}; further

reductions require the use of a different technique. The use of longer input bars with the same conical striker produced an undesirable distortion of pulse from its triangular shape as shown in Figure 30b.

III. FUTURE WORK

Th work during the interval up to February, 1973 will be devoted to completing the major objectives of the program, with certain aspects of the project requiring some additional time, as initially indicated in the original proposal. Furthermore, it has become obvious that the techniques developed will find useful applications in a broader range of problems in the field of rock mechanics than the scope of the work covered by the present proposal. Suggestions for such activities as a sequel to the current investigation will be presented in the future.

In the experimental examination of wave processes, the following endeavors are planned: (1) The development and testing of new and improved grouting materials embedded with a transducer package in a Hopkinson bar, and calibration of the unit to determine whether the discontinuities produced by drilling have been satisfactorily eliminated. (2) The drilling of deep holes in Hopkinson bars of Yule marble to simulate the installation and testing of the transducer packages in the rock blocks. (3) The improvement of the sensitivity of the transducer package by the use of ceramic IZT4 crystals that exhibit a hundredfold larger response than the quartz crystals presently employed. (4) The employment of blocks of substitute materials for simulating the drilling and embedment process of the transducers in the actual Yule marble half-spaces. (5) An extensive study of the Yule marble block geometry to locate the position of the interior transducers and their associated drilling holes in a manner so as to provide the least chance

of undesired mechanical damage to the block and, further, to provide maximum utlity for the gathering of the data and comparison with theoretical predictions. (6) The investigation of the use of transmission devices to guard against damage to the fabric of the block at the impact point. (7) Appropriate checks to establish the reproducibility of the data, and (8) Improvement of existing methods of surface measurement. Future investigations may even involve studies of the reflection processes from bounding surfaces and the effect of other types of anisotropy.

The transform analysis will be concerned with the further verification of the displacement field program, the development of more efficient routines for extracting roots of the characteristic equation to save computer time, the specification of a convolution integral procedure so as to permit utilization of the displacement field relations for an arbitrary forcing function, and the development of a separate program for the evaluation of the surface response which at present cannot be obtained as a limiting process for the body solution. In order to permit a direct comparison with experimental results, the response of the block must be predicted in terms of both local stress and strain, since the transducers employed in the experimental phase of the program measure these quantities. This requires a differentiation of the displacement field which may lead to additional numerical complications that will require resolution. It will be necessary to closely correlate the computer efforts with the experimental approach so as to permit the calculation of results at positions that are both of physical interest and experimentally accessible. The computation can be

considered to be valid only at a given station for time intervals prior to the arrival of significant reflections from bounding surfaces.

The finite element procedure will initially concentrate on a better representation of the element and studies concerned with the determination of the optimal spatial mesh density and time step size, using an isotropic medium. Upon satisfactory performance of the program in the testing phases, it will be applied to the subject problem in its most general form. Reflections from the boundary will also be considered in additional studies. It may be desirable to specialize this program for the case of plane strain in a special anisotropic medium where a closed-form solution is available for check purposes[7]. The numerical results obtained here will be compared with the corresponding information from the integral transform analysis.

The crystallographic techniques for the location of the transversely isotropic axis of the Yule marble materials will be further pursued and applied. Tensile and compressive tests under controlled dynamic conditions will be executed utilizing the concept of the mechanical converter previously described, and standard Hopkinson bar tests on the material will also be conducted on specimens parallel and perpendicular to the axis of elastic symmetry. A major effort will be required to initiate the program of fracture analysis of the material as a function of strain rate. For this purpose, the techniques developed on bone, utilizing a split Hopkinson bar, will be employed[10] and direct observation of the fracture process by means of high-speed photography will be sought. The tracing of the crack propagation by means of transmitted light effects will also be attempted.

The ultimate goal of this portion of the investigation will be the complete characterization of the mechanical response of this material to loads ranging in rate from the quasi-static to the impact domain. This will hopefully be accomplished by a model that incorporates the major features observed during the current experimental program.

LIST OF FIGURES

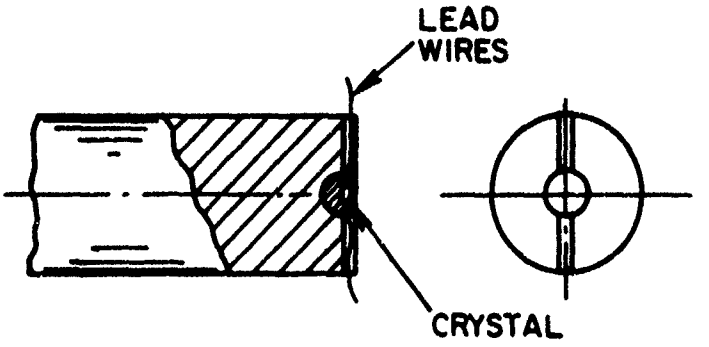

Fig. 1

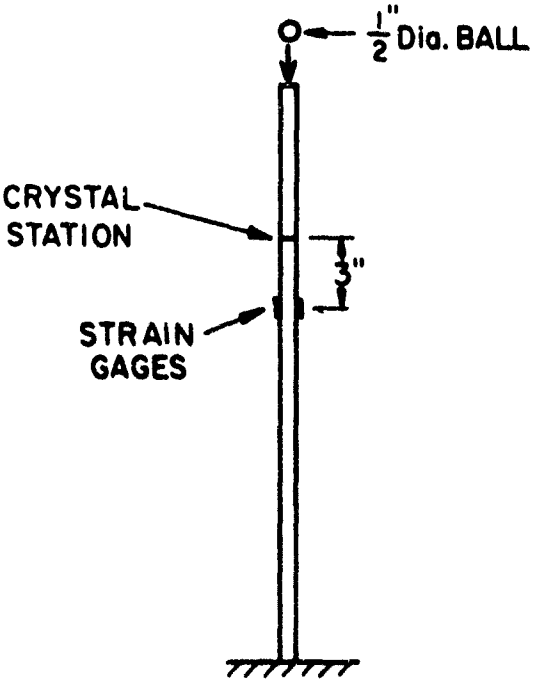

Fig. 2

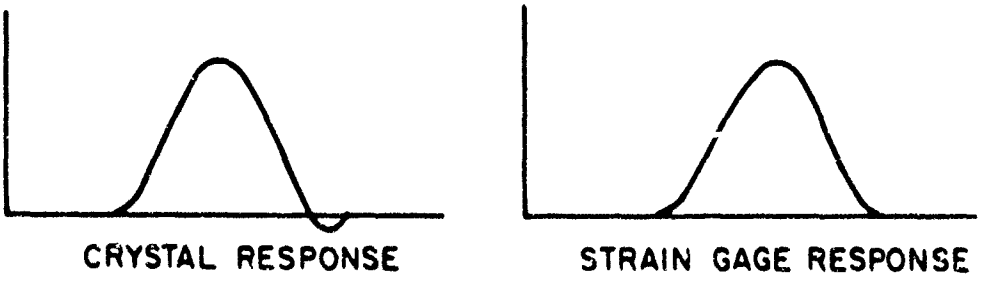

Fig. 3

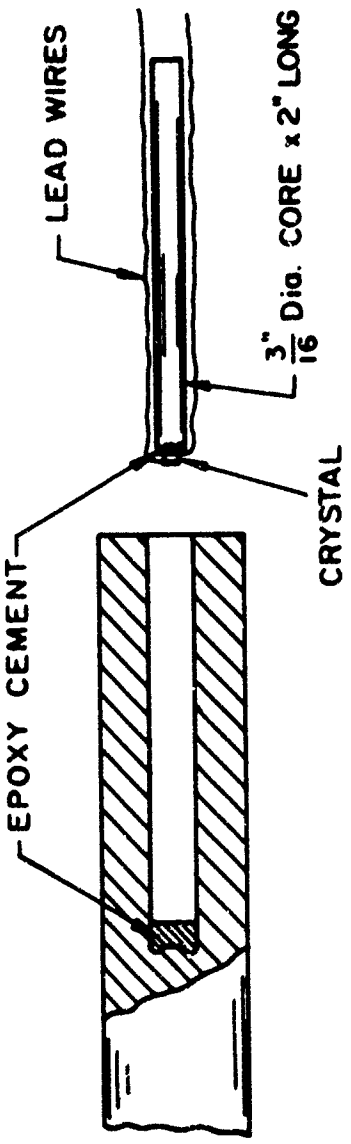
LEAD WIRES
3/16" Dia. CORE x 2" LONG
CRYSTAL
EPOXY CEMENT

Fig. 4

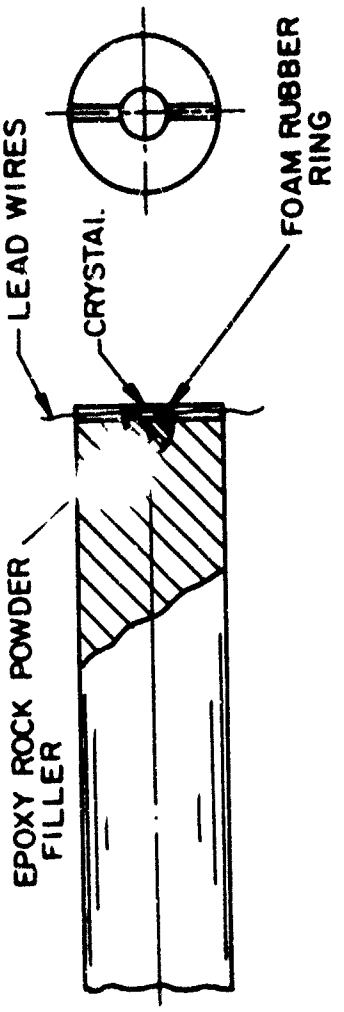
LEAD WIRES
CRYSTAL
FOAM RUBBER RING
EPOXY ROCK POWDER FILLER

Fig. 5

20 μsec/div.

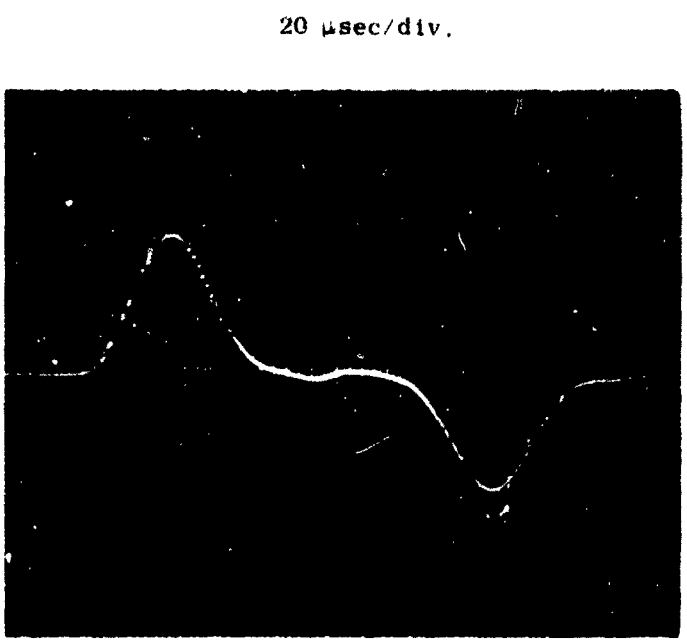

0.5 mV/div.

Fig. 6a

20 μsec/div.

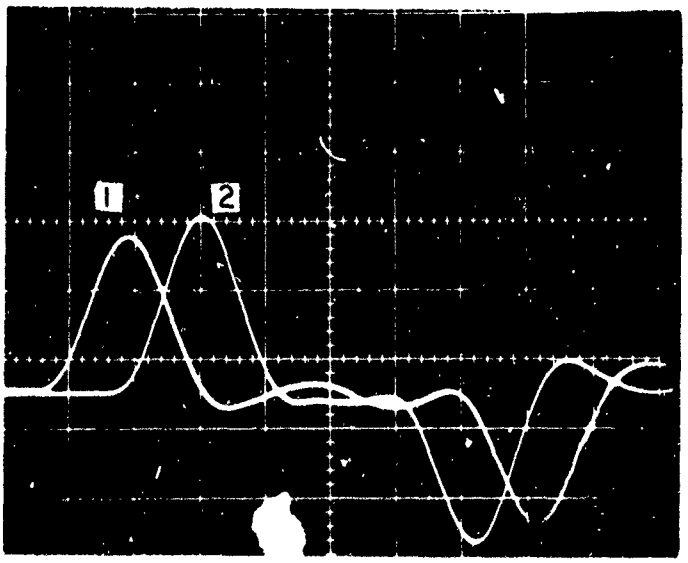

20 mV/div.

(1) Response of totally embedded crystal.
(2) Response of laterally unconstrained crystal.

Fig. 6b

20 μsec/div.

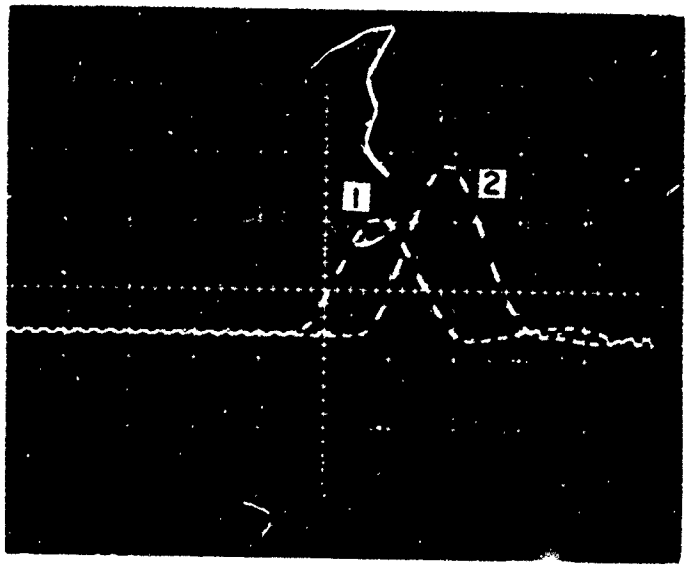

20 mV/div.

(1) Response of totally embedded crystal.
(2) Response of laterally unconstrained crystal.

Fig. 7

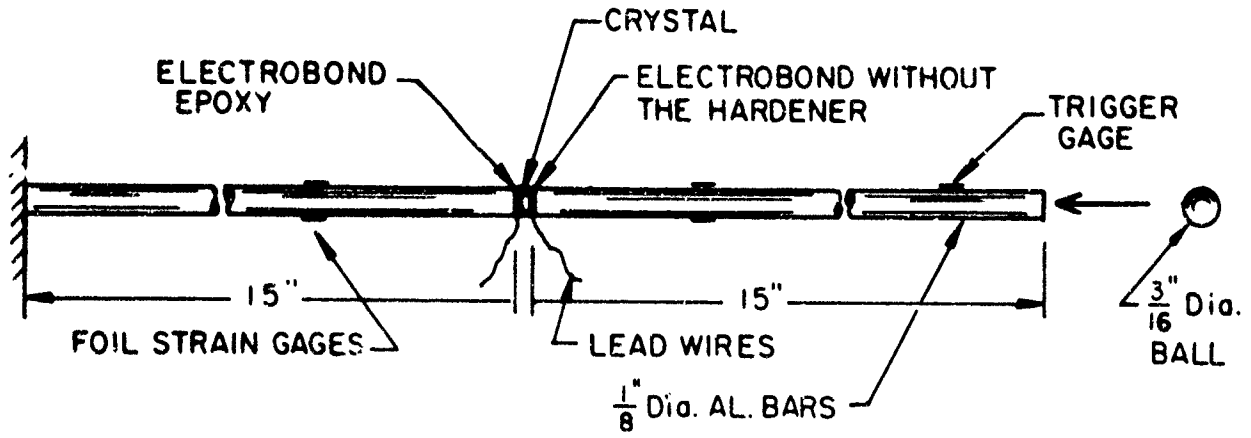

Fig. 8

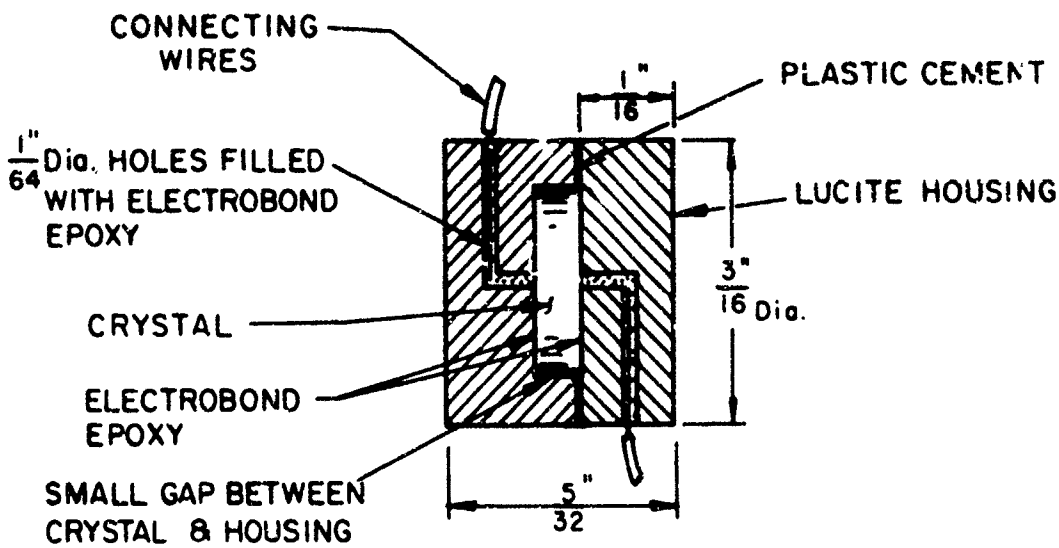
CONNECTING WIRES
1/16"
PLASTIC CEMENT
1/64" Dia. HOLES FILLED WITH ELECTROBOND EPOXY
LUCITE HOUSING
3/16" Dia.
CRYSTAL
ELECTROBOND EPOXY
SMALL GAP BETWEEN CRYSTAL & HOUSING
5/32"

Fig. 9

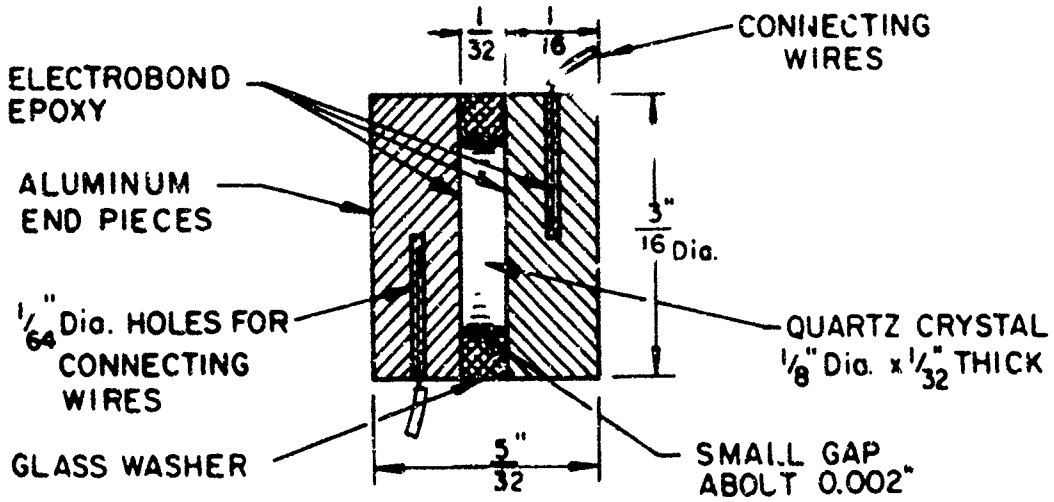
1/32
1/16
CONNECTING WIRES
ELECTROBOND EPOXY
ALUMINUM END PIECES
3/16" Dia.
1/64" Dia. HOLES FOR CONNECTING WIRES
QUARTZ CRYSTAL 1/8" Dia. x 1/32" THICK
GLASS WASHER
5/32"
SMALL GAP ABOUT 0.002"

Fig. 10

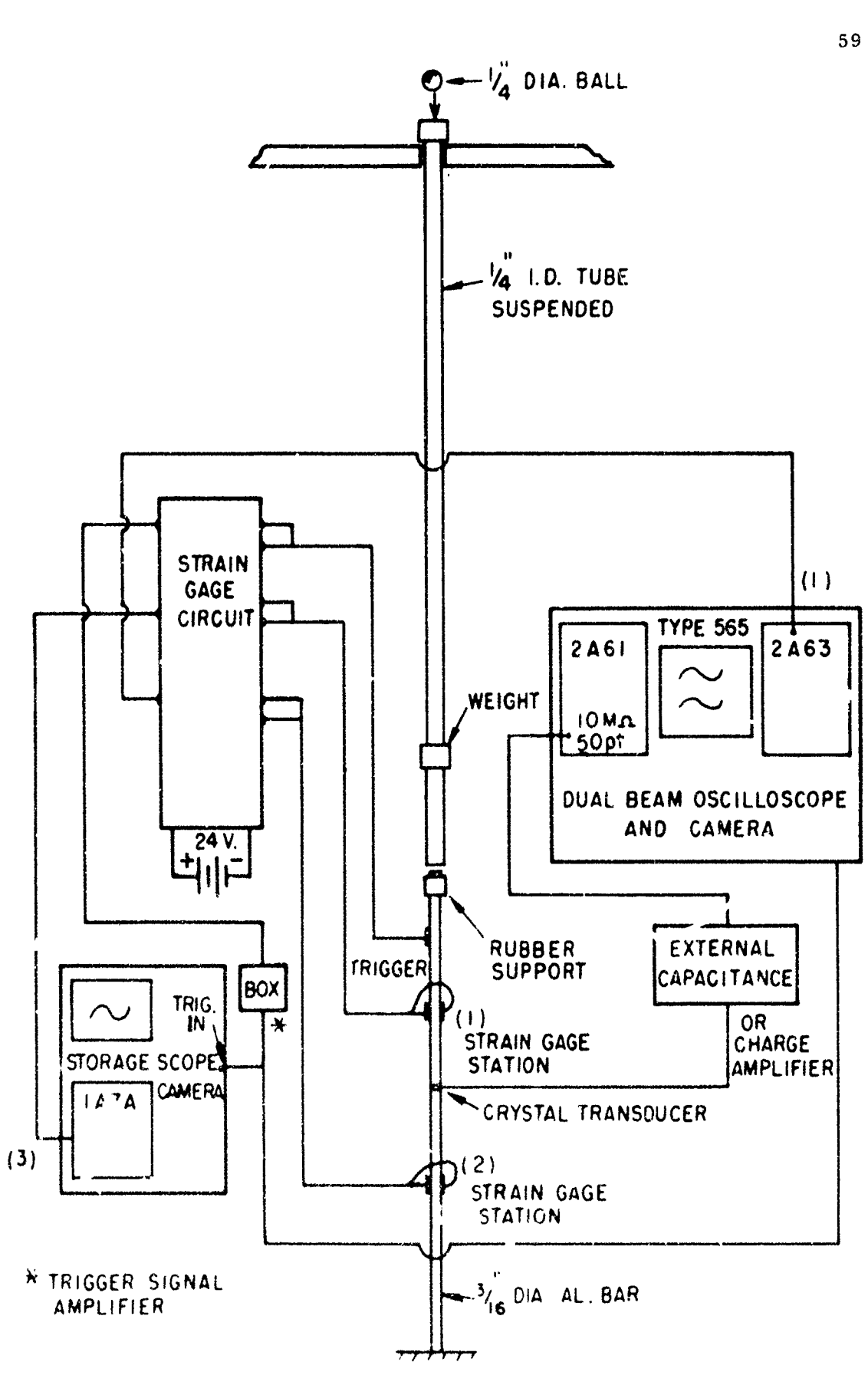
1/4" DIA. BALL
1/4" I.D. TUBE SUSPENDED
STRAIN GAGE CIRCUIT
24 V.
(1)
TYPE 565
2A61
10MΩ 50pf
2A63
DUAL BEAM OSCILLOSCOPE AND CAMERA
WEIGHT
RUBBER SUPPORT
TRIGGER
EXTERNAL CAPACITANCE
OR CHARGE AMPLIFIER
BOX
*
TRIG. IN
STORAGE SCOPE
CAMERA
(3)
(1) STRAIN GAGE STATION
CRYSTAL TRANSDUCER
(2) STRAIN GAGE STATION
* TRIGGER SIGNAL AMPLIFIER
3/16" DIA AL. BAR

10 μsec/div.

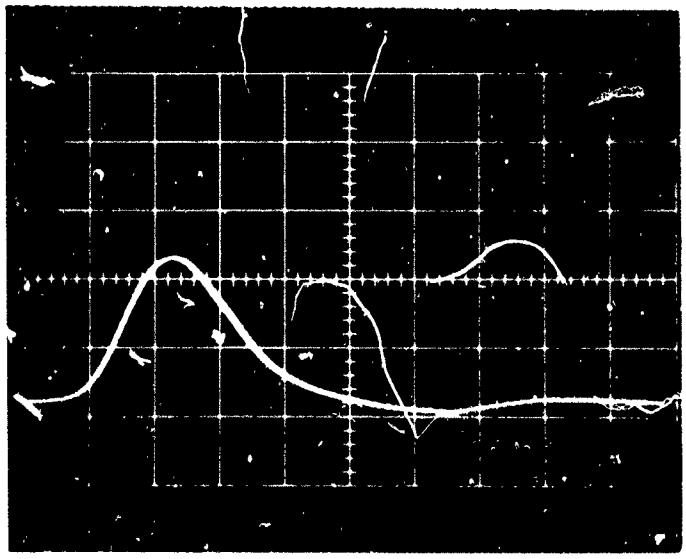

1mV/div.

Response of
Strain Gage 1

Fig. 12a

10 μsec/div.

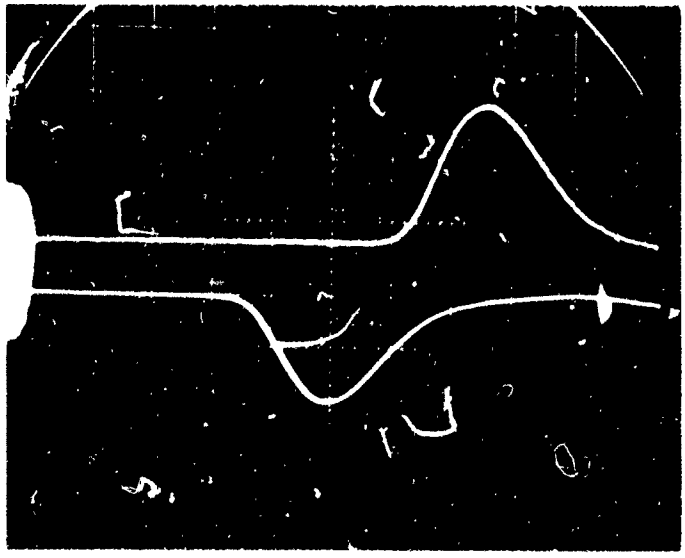

Response of
Strain Gage 2
1mV div.

Crystal Response
20mV div.

Fig. 12b

10 μsec/div.

0.1V/div.

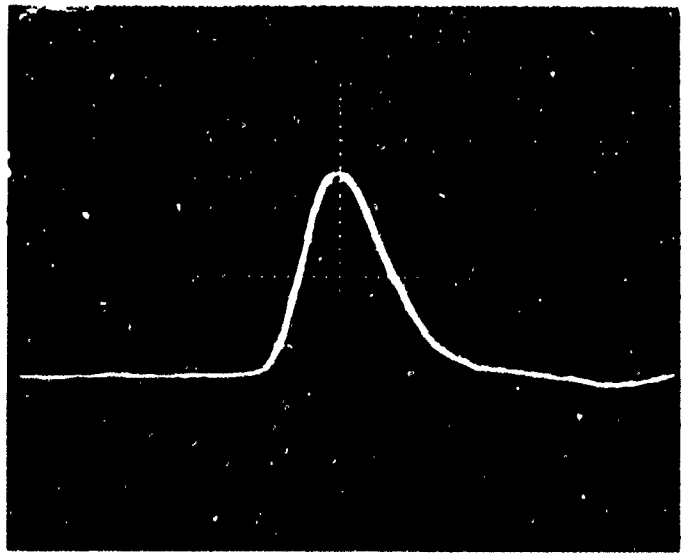

Crystal Response

Fig. 13a

10 μsec/div.

1mV/div

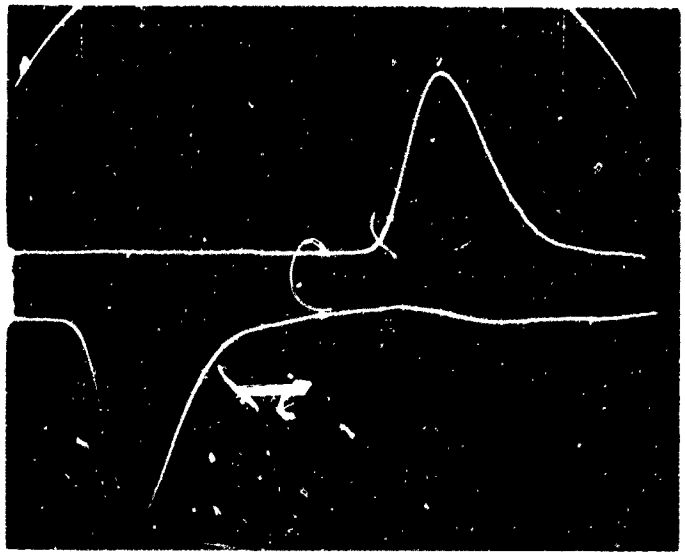

Strain gage 2

Strain gage 1

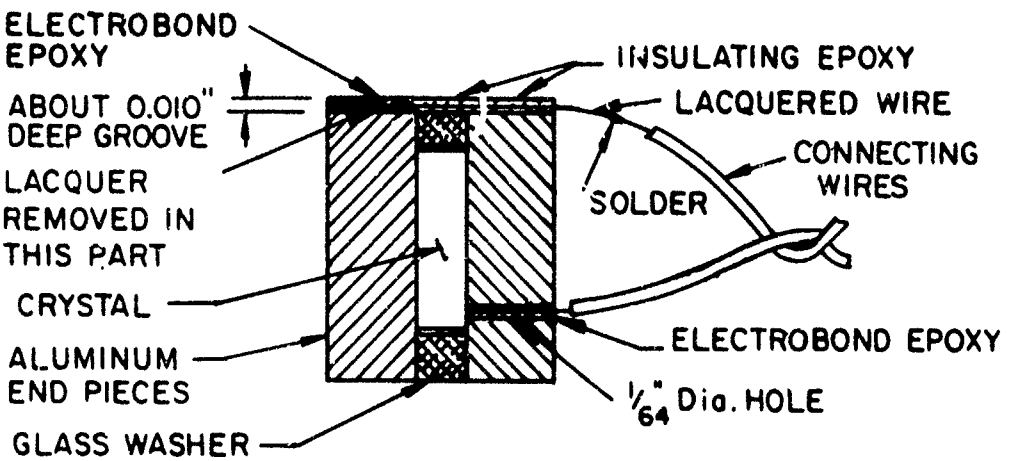
ELECTROBOND EPOXY
ABOUT 0.010" DEEP GROOVE
LACQUER REMOVED IN THIS PART
CRYSTAL
ALUMINUM END PIECES
GLASS WASHER
INSULATING EPOXY
LACQUERED WIRE
CONNECTING WIRES
SOLDER
ELECTROBOND EPOXY
1/64" Dia. HOLE

Fig. 14

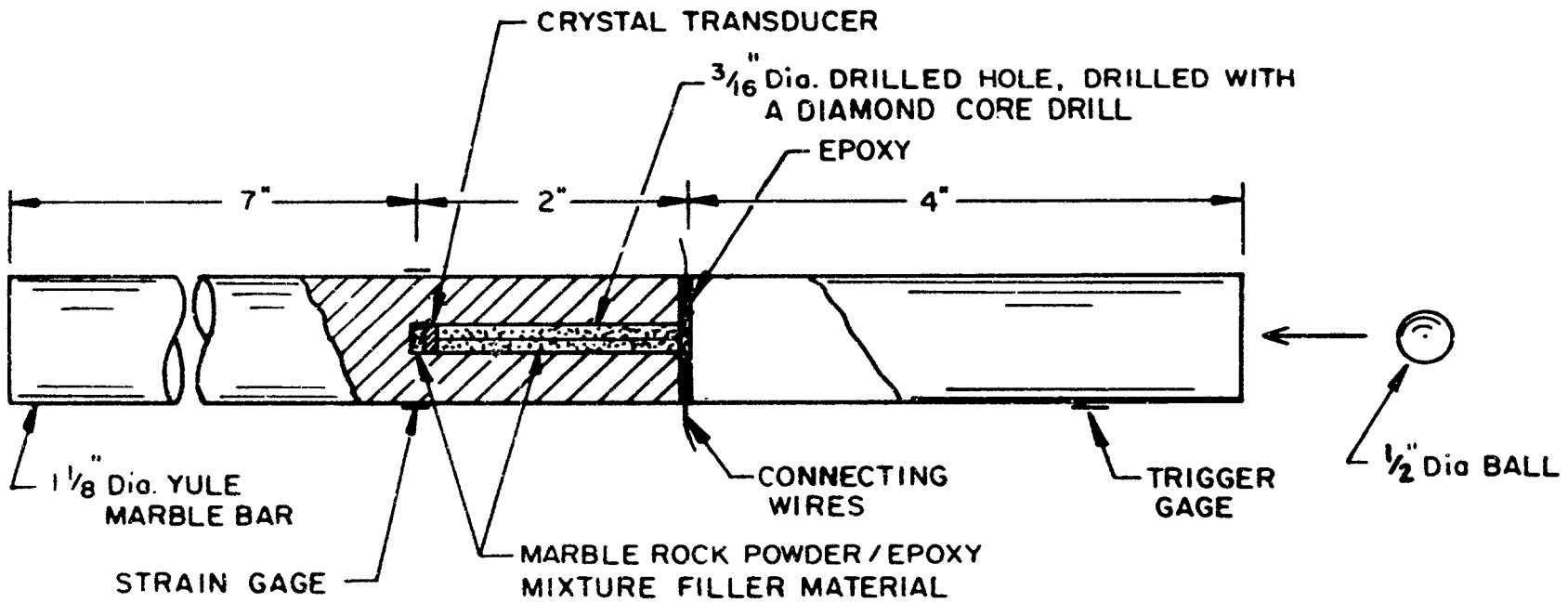
CRYSTAL TRANSDUCER
3/16" Dia. DRILLED HOLE, DRILLED WITH A DIAMOND CORE DRILL
EPOXY
7"
2"
4"
1 1/8" Dia. YULE MARBLE BAR
STRAIN GAGE
MARBLE ROCK POWDER / EPOXY MIXTURE FILLER MATERIAL
CONNECTING WIRES
TRIGGER GAGE
1/2" Dia BALL

Fig. 15

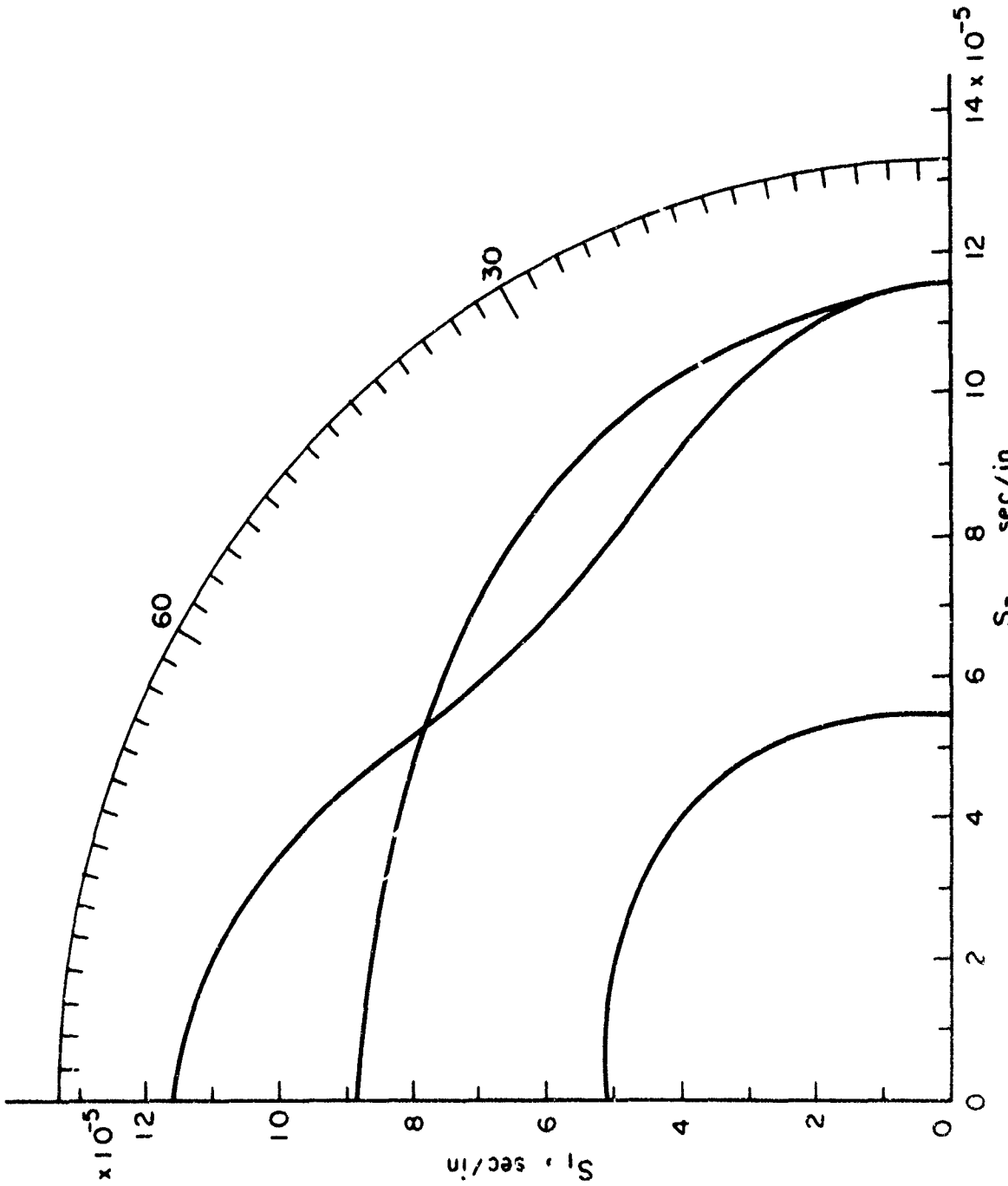

Fig. 16

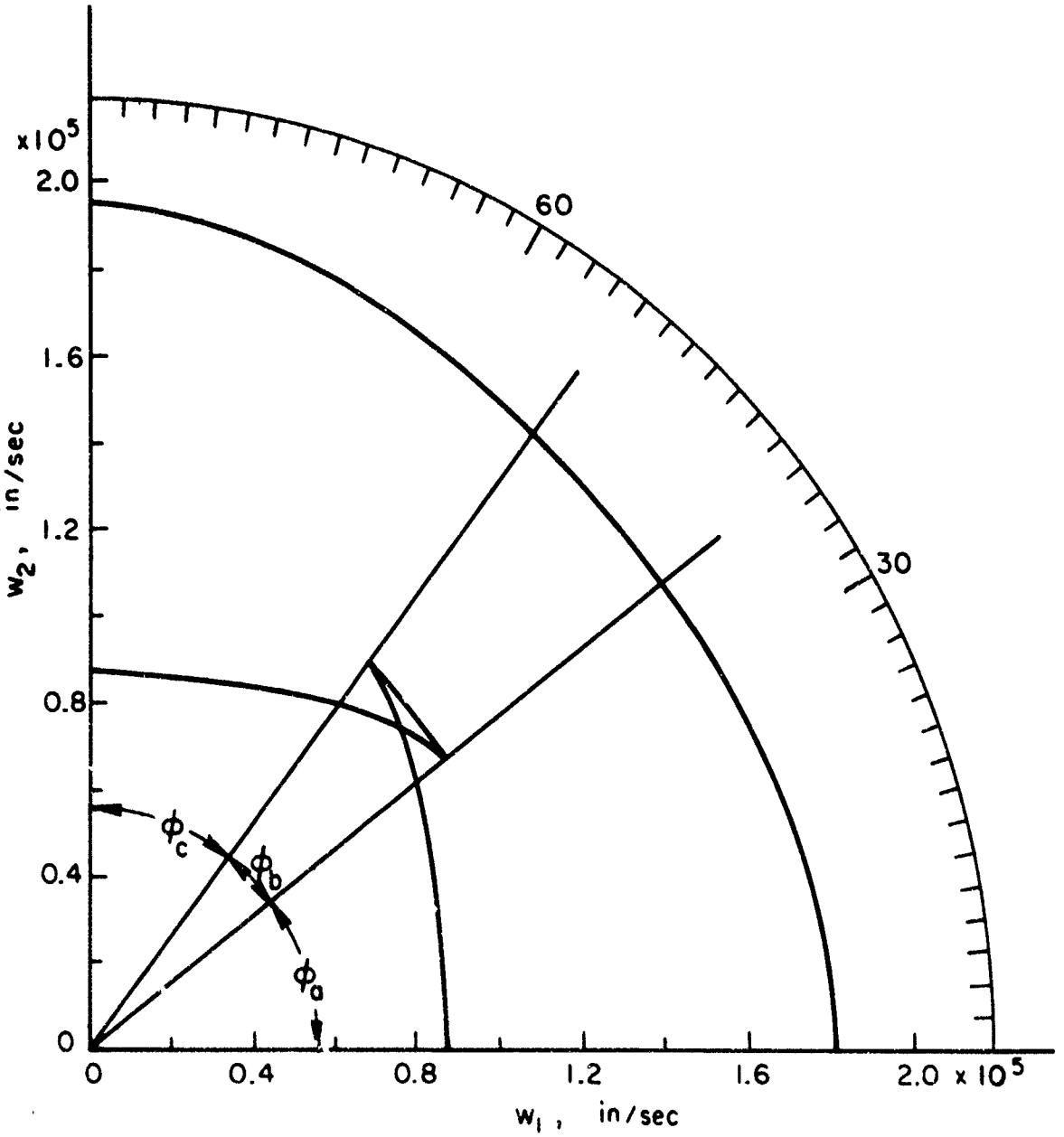
x10^5
2.0
1.6
1.2
0.8
0.4
0
w_2, in/sec
60
30
ϕ_c
ϕ_b
ϕ_a
0
0.4
0.8
1.2
1.6
2.0 x 10^5
w_1, in/sec

Fig. 17

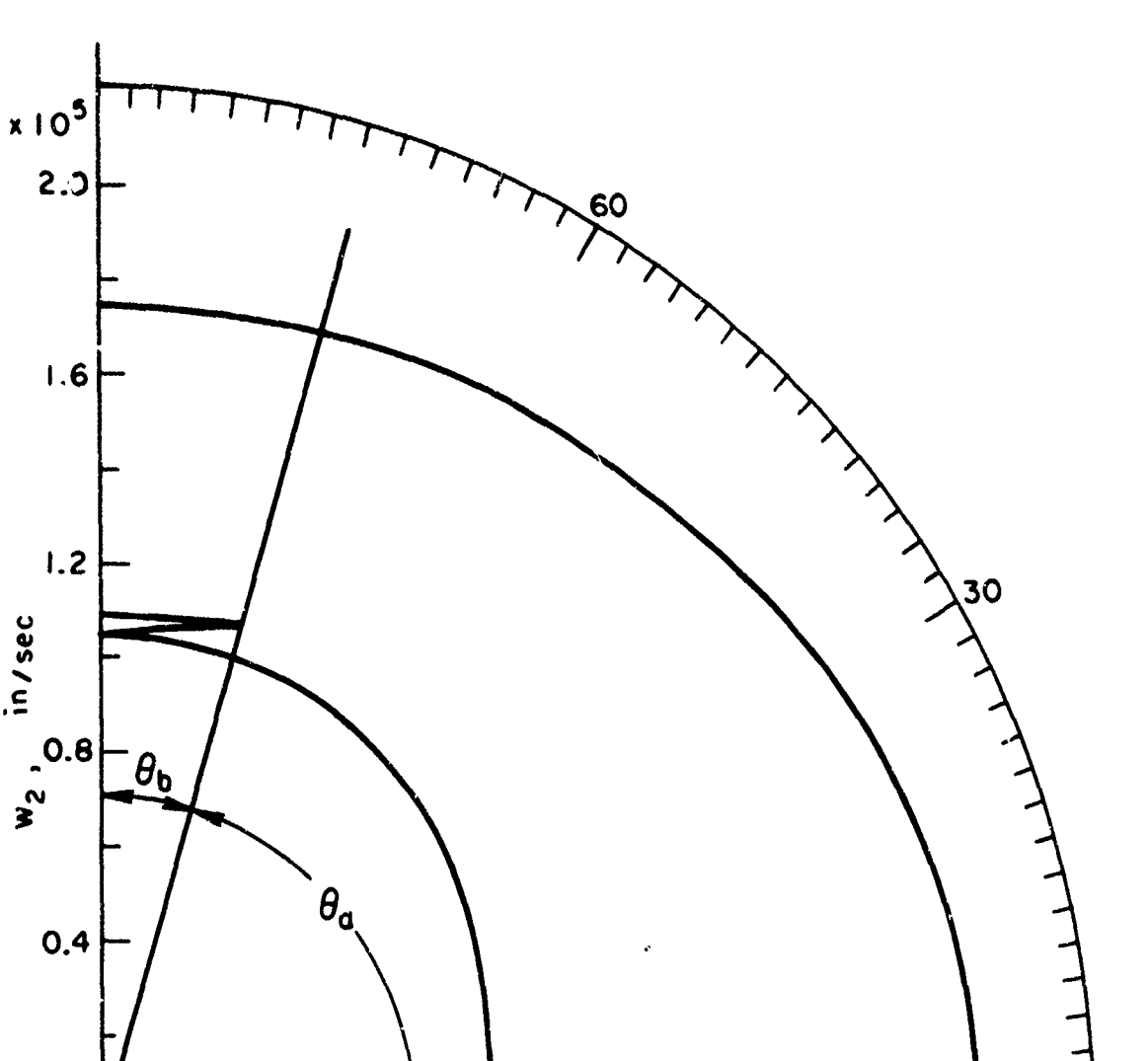
x 10^5
2.0
1.6
1.2
0.8
0.4
0
w2 , in/sec
60
30
θb
θa
0
0.4
0.8
1.2
1.6
2.0 x 10^5
w1 , in/sec

Fig. 18

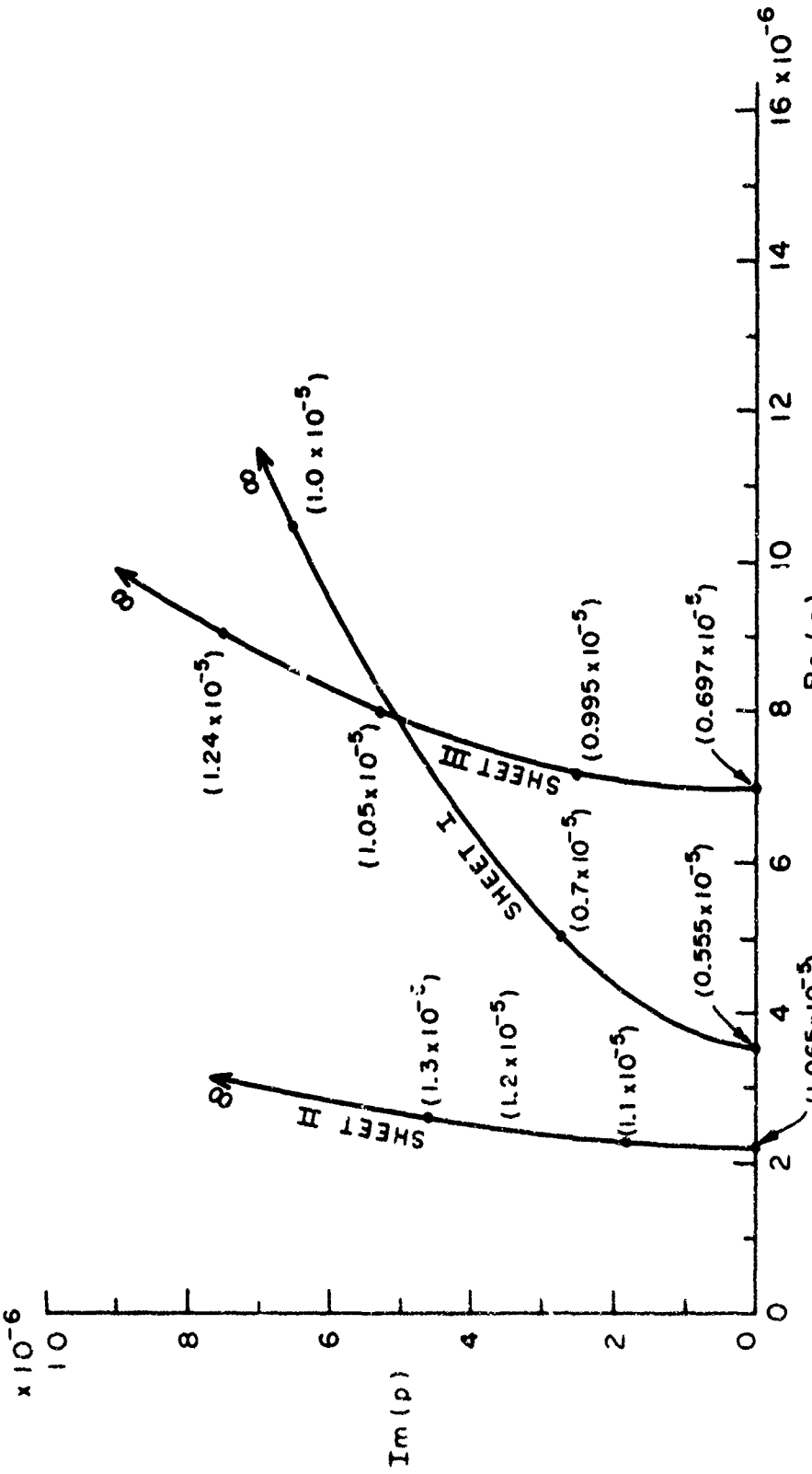
Im (p)
Re (p)
x 10^-6
SHEET II
SHEET I
SHEET III
(1.3x10^-5)
(1.2x10^-5)
(1.1x10^-5)
(1.24x10^-5)
(1.05x10^-5)
(1.0x10^-5)
(0.7x10^-5)
(0.555x10^-5)
(1.065x10^-5)
(0.995x10^-5)
(0.697x10^-5)

Fig. 19

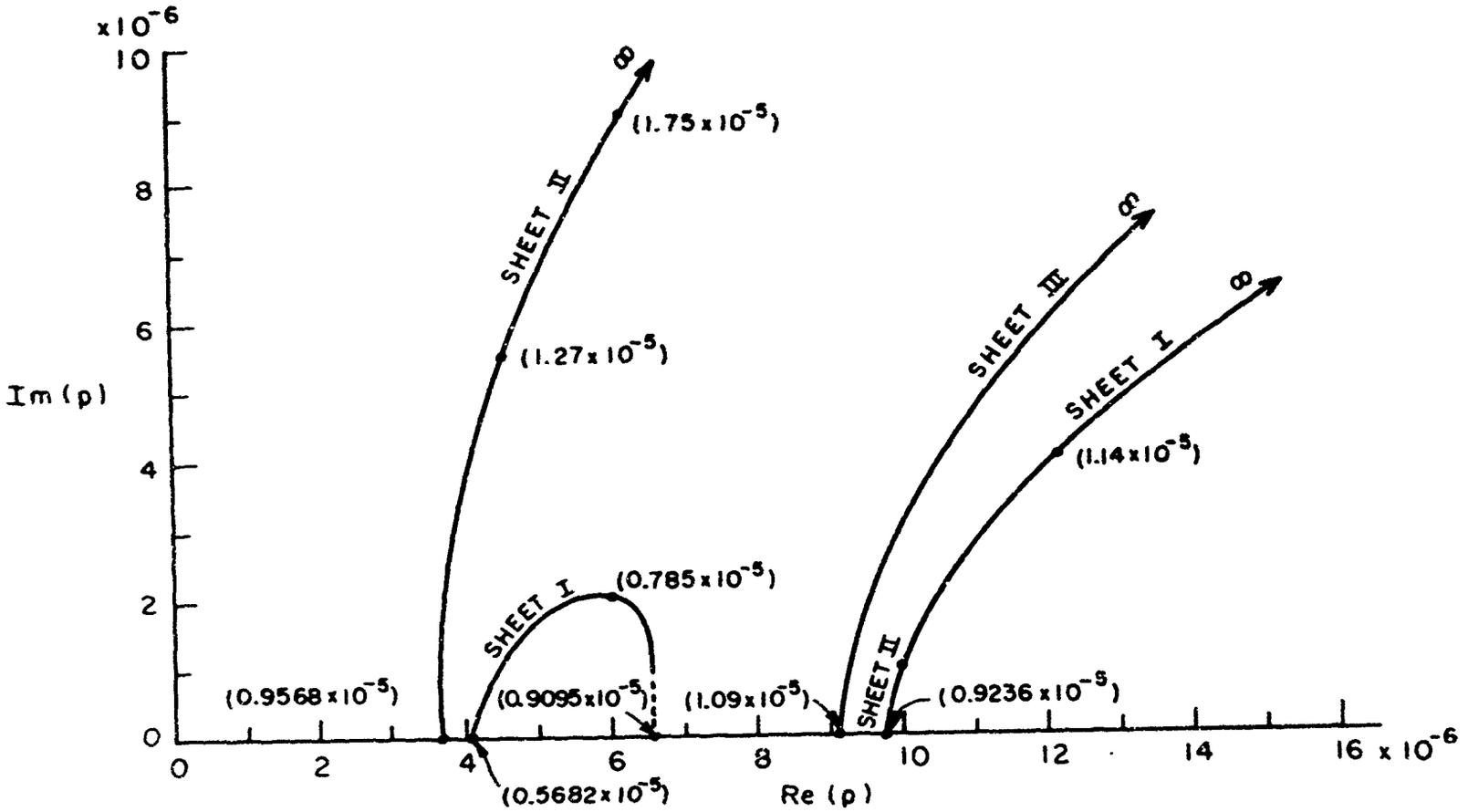
x10^-6
10
8
6
4
2
0
Im(ρ)
0
2
4
6
8
10
12
14
16 x 10^-6
Re(ρ)
SHEET II
(1.75x10^-5)
(1.27x10^-5)
SHEET I
(0.785x10^-5)
(0.9568x10^-5)
(0.9095x10^-5)
(0.5682x10^-5)
SHEET III
(1.09x10^-5)
SHEET II
(0.9236x10^-5)
SHEET I
(1.14x10^-5)

Fig. 20

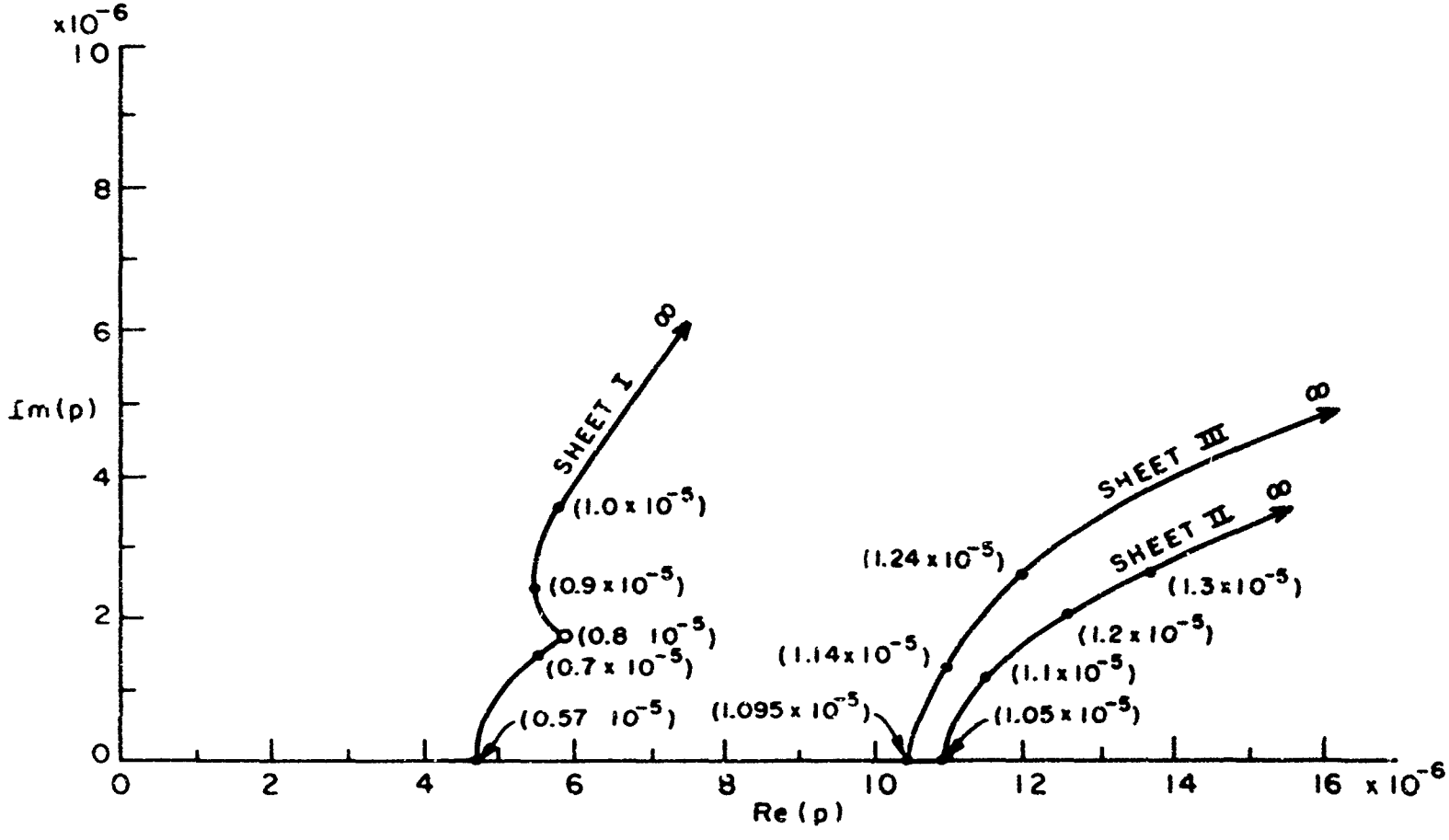
x10^-6
10
8
6
4
2
0
Im(p)
0
2
4
6
8
10
12
14
16 x 10^-6
Re(p)
SHEET I
∞
(1.0 x 10^-5)
(0.9 x 10^-5)
(0.8 10^-5)
(0.7 x 10^-5)
(0.57 10^-5)
SHEET III
∞
(1.24 x 10^-5)
(1.14 x 10^-5)
(1.095 x 10^-5)
SHEET II
∞
(1.3 x 10^-5)
(1.2 x 10^-5)
(1.1 x 10^-5)
(1.05 x 10^-5)

Fig. 21

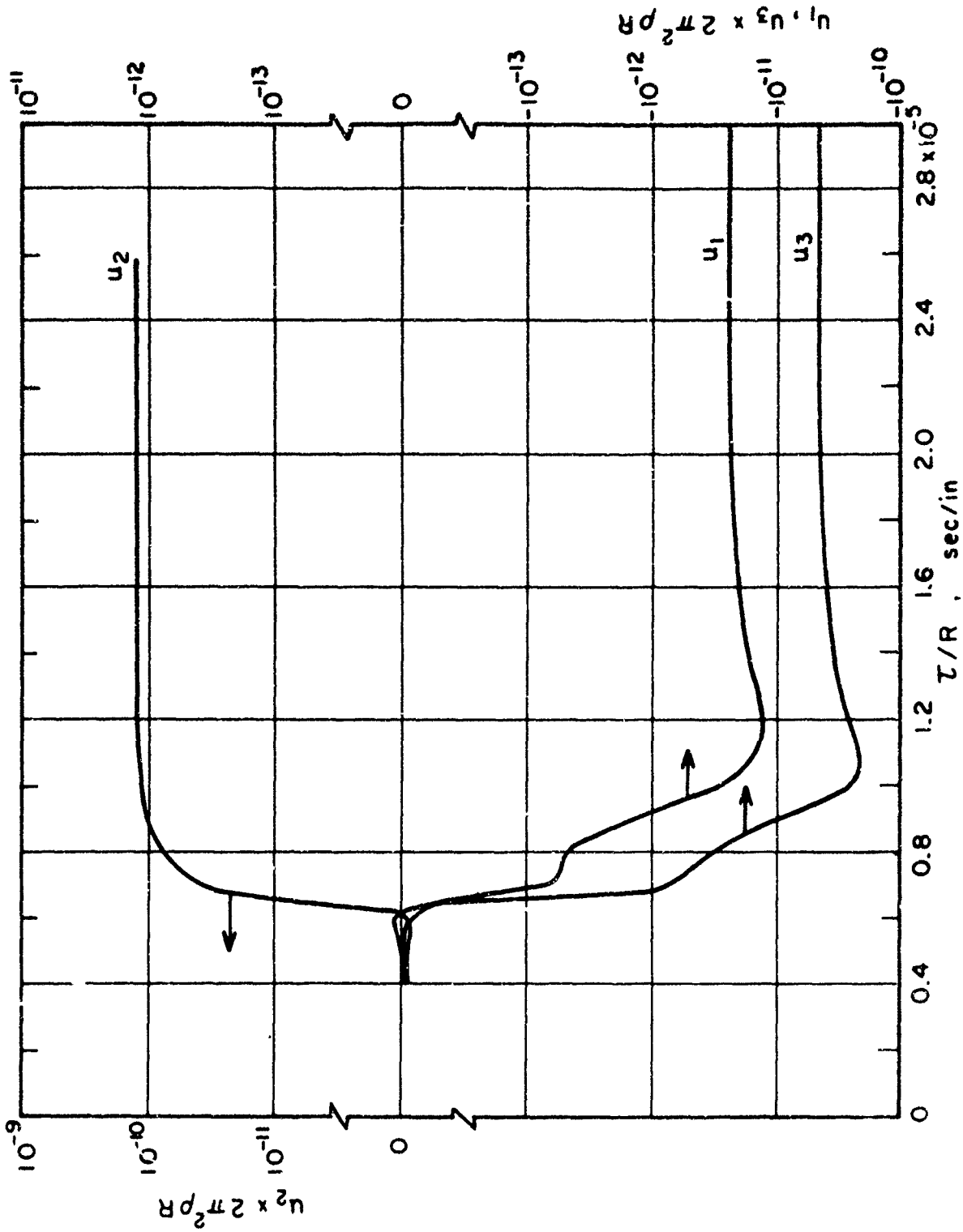
$u_1, u_3 \times 2\pi^2 \rho R$
10^{-11}
10^{-12}
10^{-13}
0
-10^{-13}
-10^{-12}
-10^{-11}
-10^{-10}
2.8×10^{-5}
u_2
u_1
u_3
2.4
2.0
1.6
1.2
τ/R , sec/in
0.8
0.4
0
10^{-9}
10^{-10}
10^{-11}
0
$u_2 \times 2\pi^2 \rho R$

Fig. 22

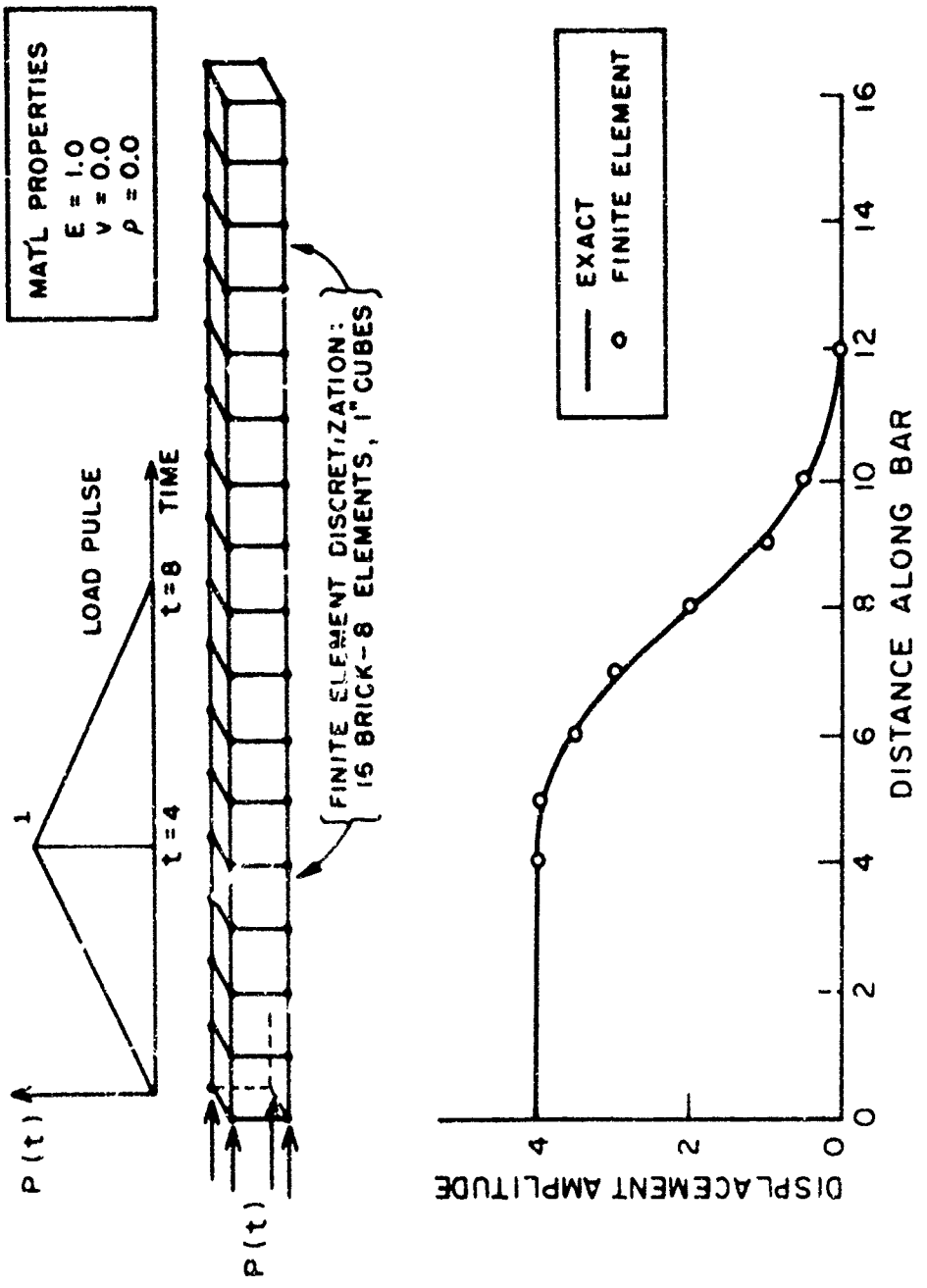
MATL PROPERTIES
E = 1.0
ν = 0.0
ρ = 0.0
LOAD PULSE
TIME
t=8
t=4
1
P(t)
FINITE ELEMENT DISCRETIZATION:
15 BRICK-8 ELEMENTS, 1" CUBES
P(t)
EXACT
FINITE ELEMENT
DISPLACEMENT AMPLITUDE
4
2
0
0
2
4
6
8
10
12
14
16
DISTANCE ALONG BAR

Fig. 23

COMMON PROPERTIES FOR ALL MODELS	
YOUNGS MODULUS,	E = 2.50
POISSONS RATIO	ν = 0.25
MATERIAL DENSITY	ρ = 1.00
LOADING	P(t) = 1 (sin 2πt), 0<t< 0.5
	P(t) = 0, OTHERWISE

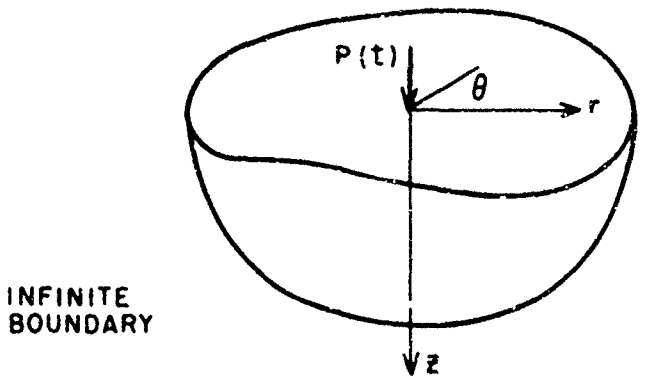

(a)

INFINITE BOUNDARY

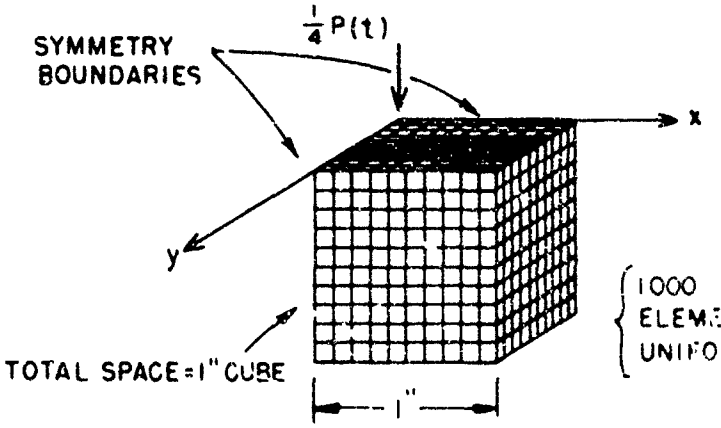

(b)

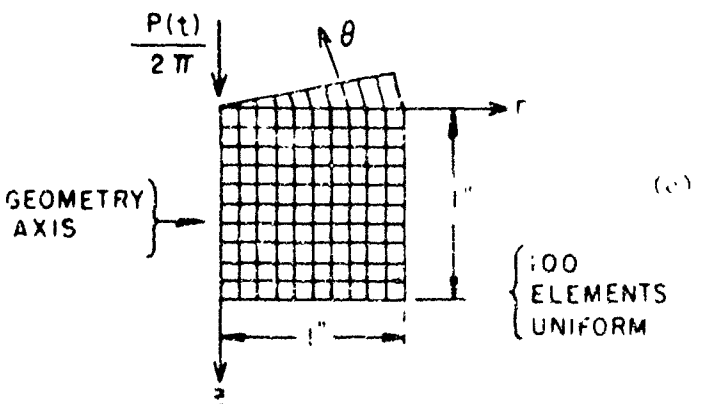

(c)

TOTAL SPACE IS 1" x 1" x 1 RADIAN

FIG. 24

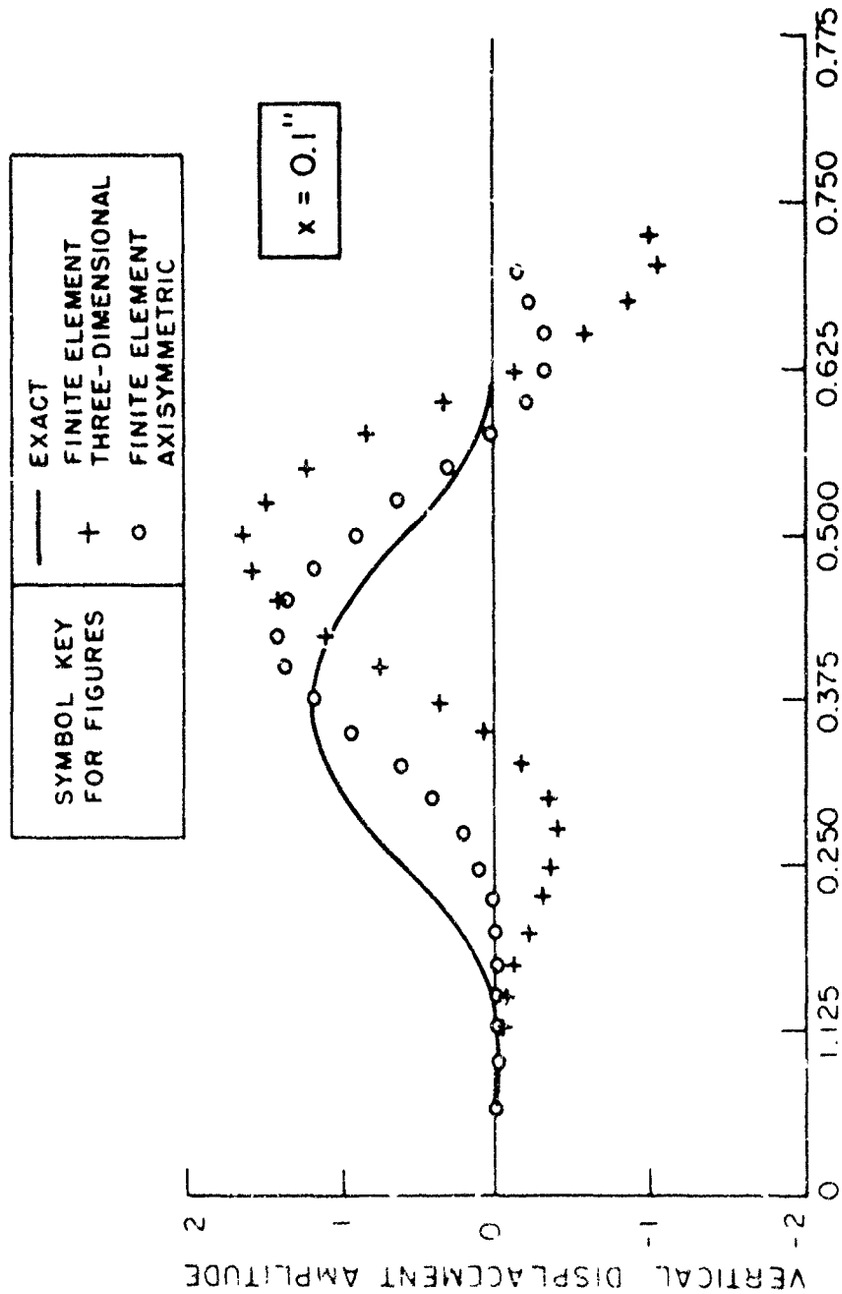
SYMBOL KEY FOR FIGURES
EXACT
FINITE ELEMENT THREE-DIMENSIONAL
FINITE ELEMENT AXISYMMETRIC
x = 0.1"
VERTICAL DISPLACEMENT AMPLITUDE
2
1
0
-1
-2
0
0.125
0.250
0.375
0.500
0.625
0.750
0.775
t, TIME, seconds

Fig. 25a

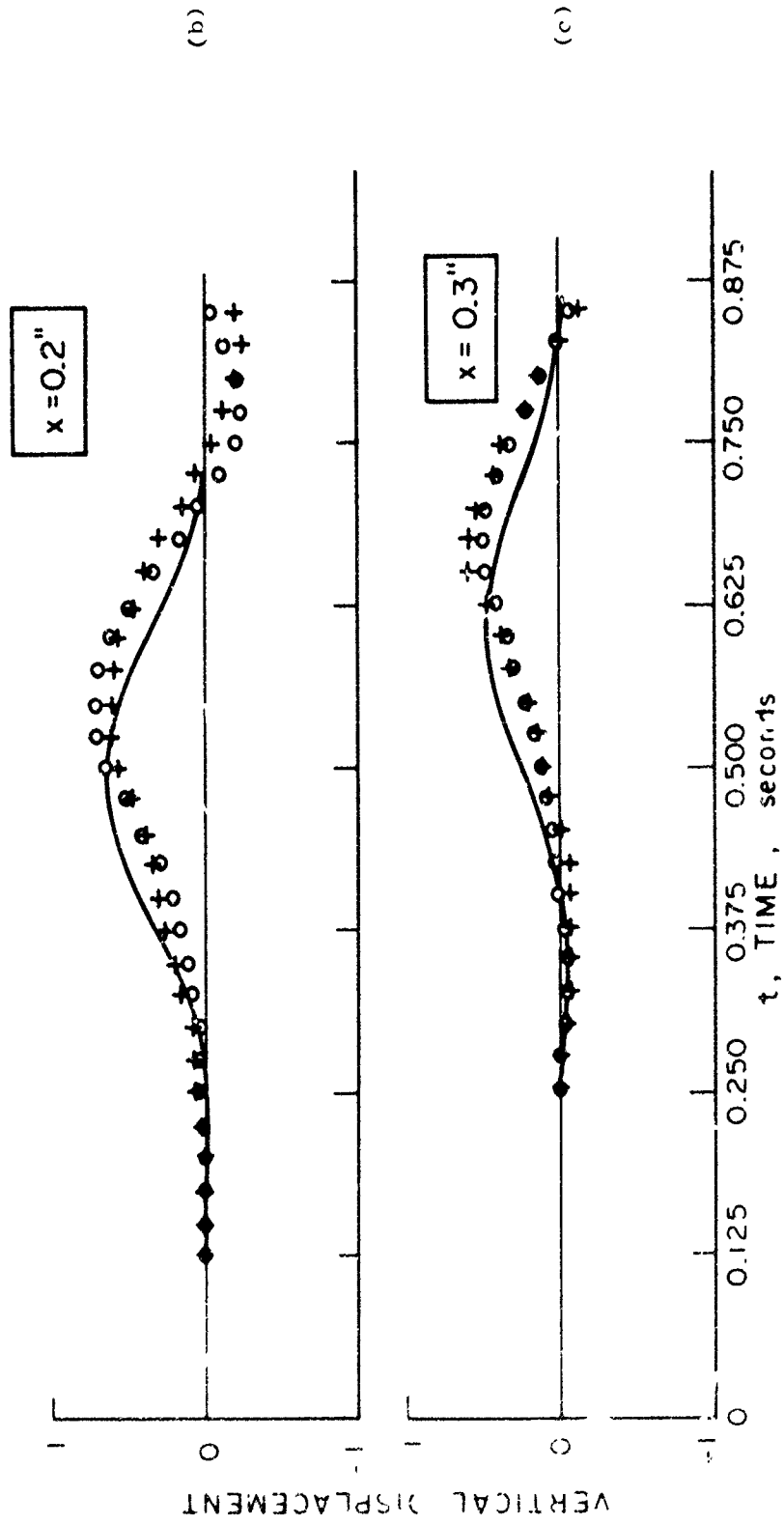
(b)
(c)
x=0.2"
x=0.3"
VERTICAL DISPLACEMENT
1
0
-1
0
0.125
0.250
0.375
0.500
0.625
0.750
0.875
t, TIME, seconds

FIG. 23

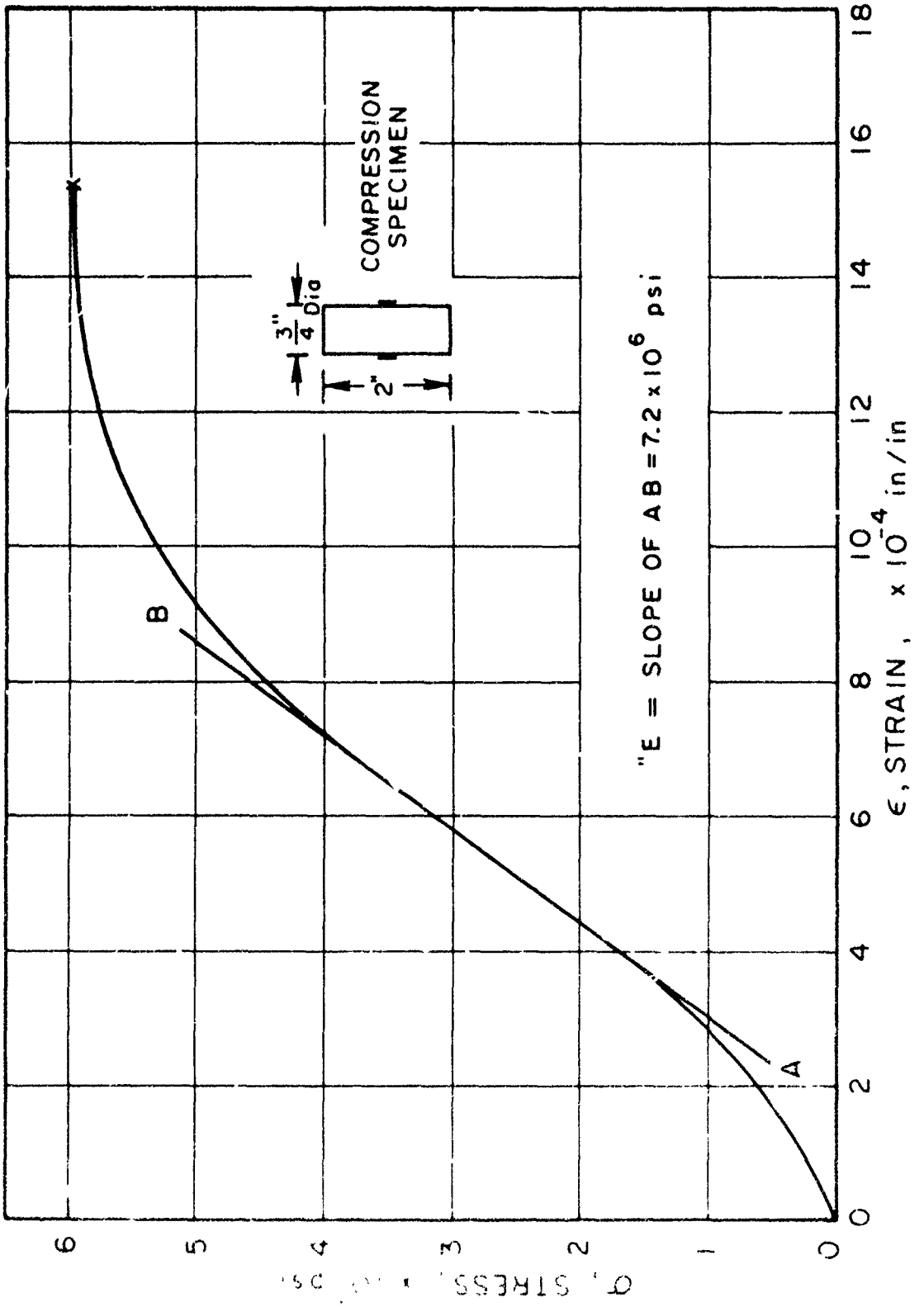
COMPRESSION SPECIMEN
3/4" Dia
2"
B
A
"E = SLOPE OF AB = 7.2 x 10^6 psi
ε, STRAIN, x 10^-4 in/in
σ, STRESS, x 10^3 psi
0
2
4
6
8
10
12
14
16
18
1
3
5

Fig. 26

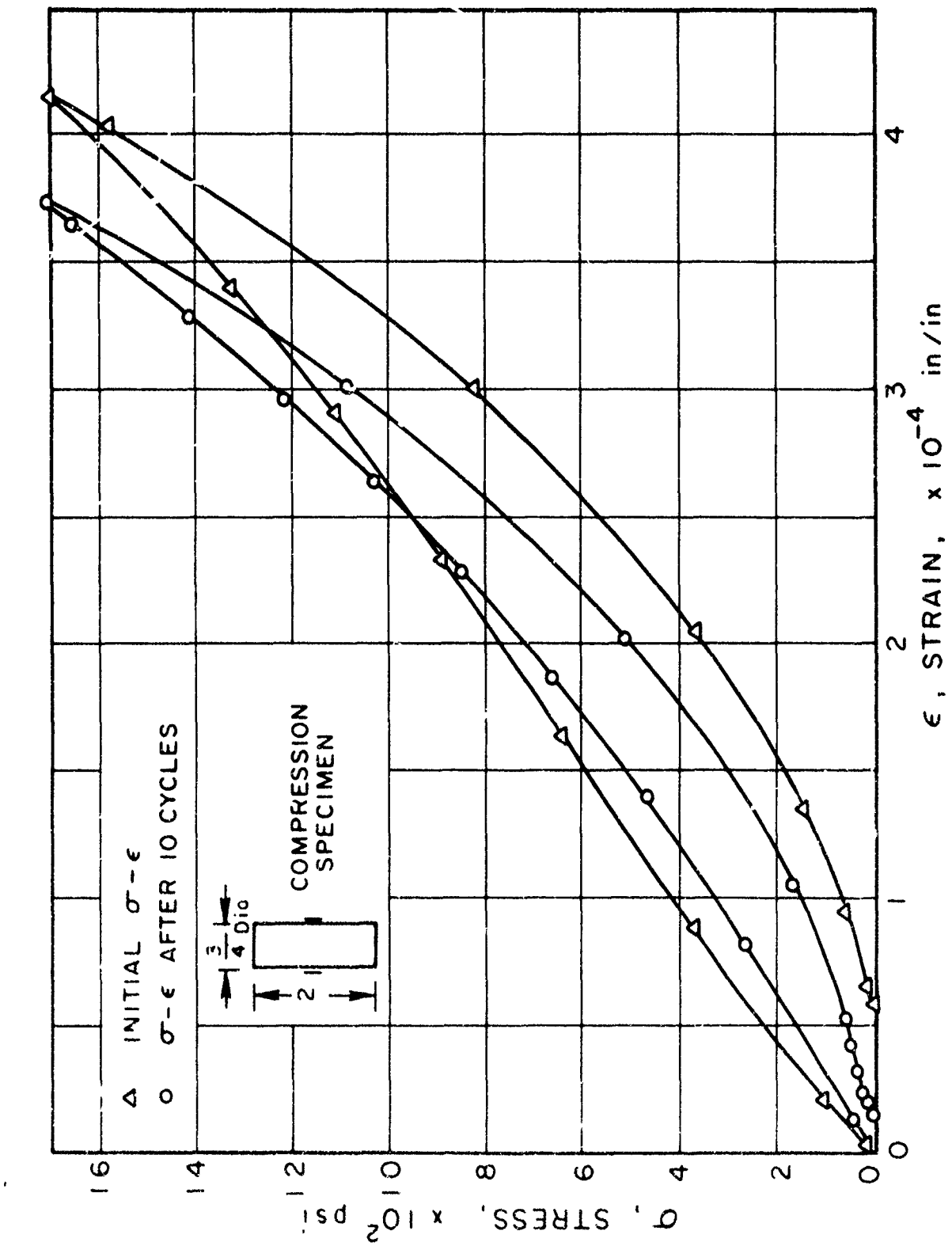
σ, STRESS, x 10² psi
ε, STRAIN, x 10⁻⁴ in/in
Δ INITIAL σ-ε
o σ-ε AFTER 10 CYCLES
COMPRESSION SPECIMEN
2
¾ Dia

Fig. 27

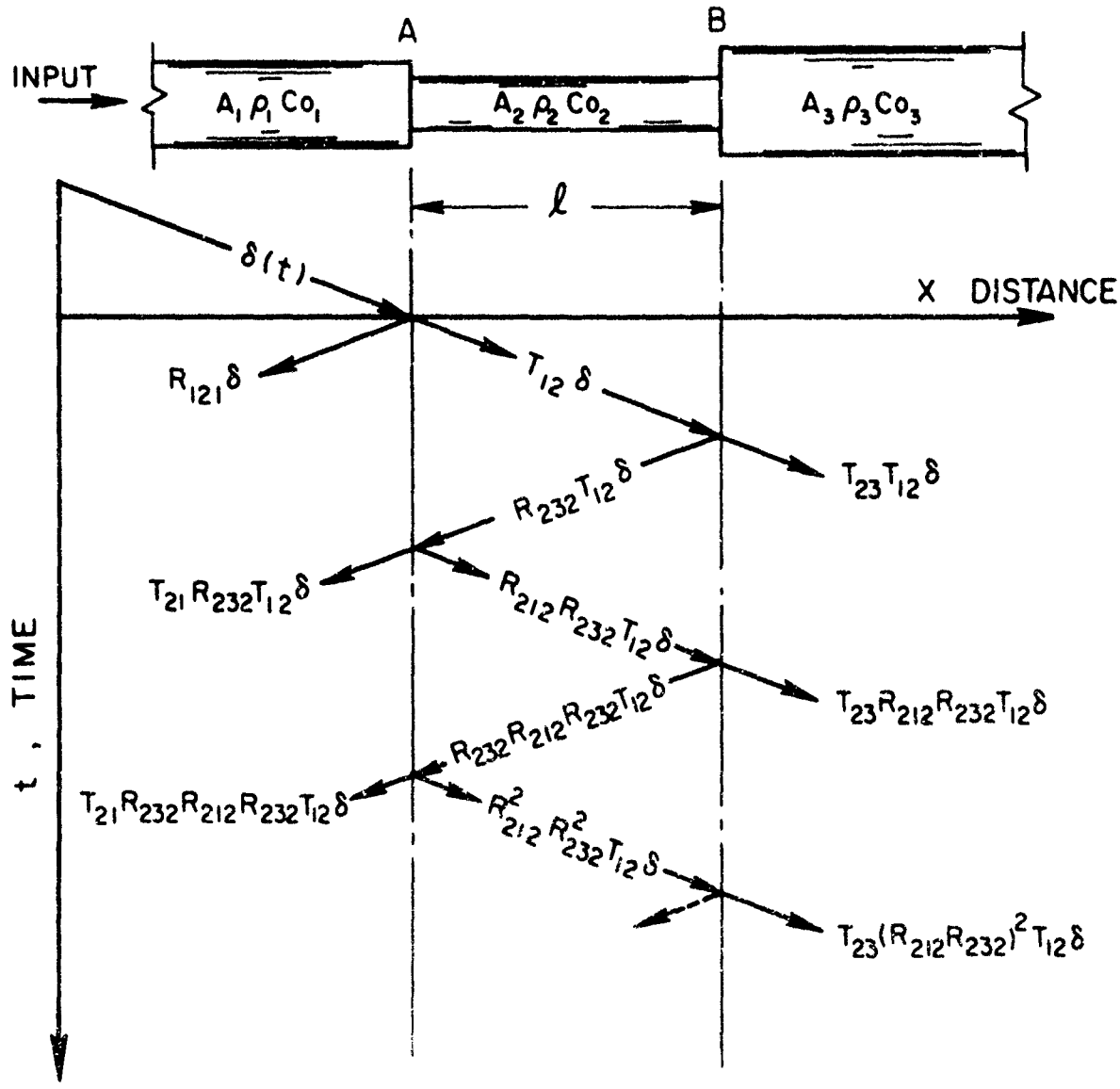
A
B
INPUT
$A_1 \rho_1 Co_1$
$A_2 \rho_2 Co_2$
$A_3 \rho_3 Co_3$
ℓ
$\delta(t)$
X DISTANCE
$R_{121}\delta$
$T_{12}\delta$
$T_{23}T_{12}\delta$
$R_{232}T_{12}\delta$
$T_{21}R_{232}T_{12}\delta$
$R_{212}R_{232}T_{12}\delta$
$T_{23}R_{212}R_{232}T_{12}\delta$
$R_{232}R_{212}R_{232}T_{12}\delta$
$T_{21}R_{232}R_{212}R_{232}T_{12}\delta$
$R_{212}^2 R_{232}^2 T_{12}\delta$
$T_{23}(R_{212}R_{232})^2 T_{12}\delta$
t , TIME

FIG. 28

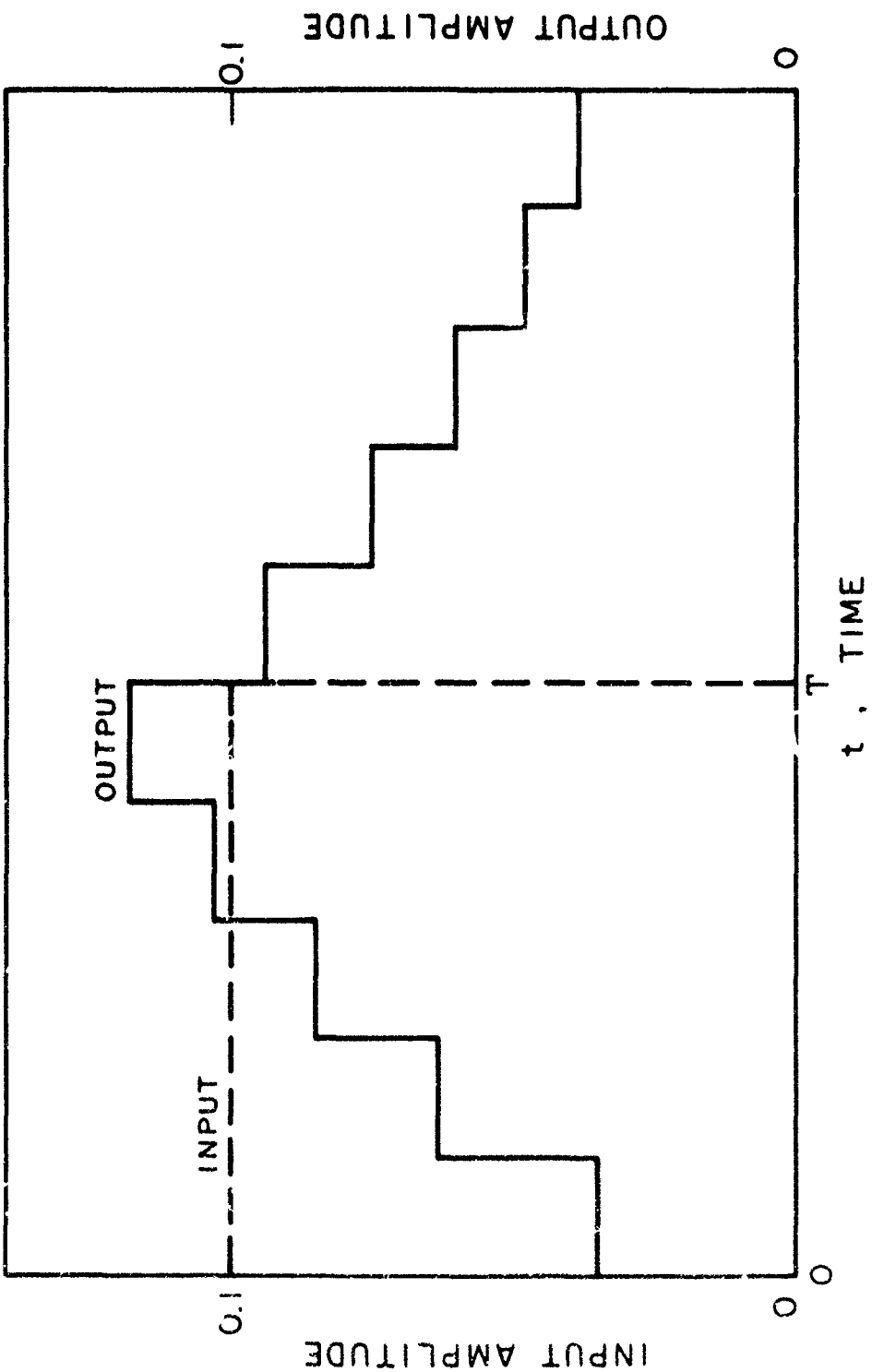
OUTPUT AMPLITUDE
1.0
0
OUTPUT
INPUT
T
t , TIME
0.1
0
INPUT AMPLITUDE

Fig. 29

100 μsec/div.

535 μin/in/d v.

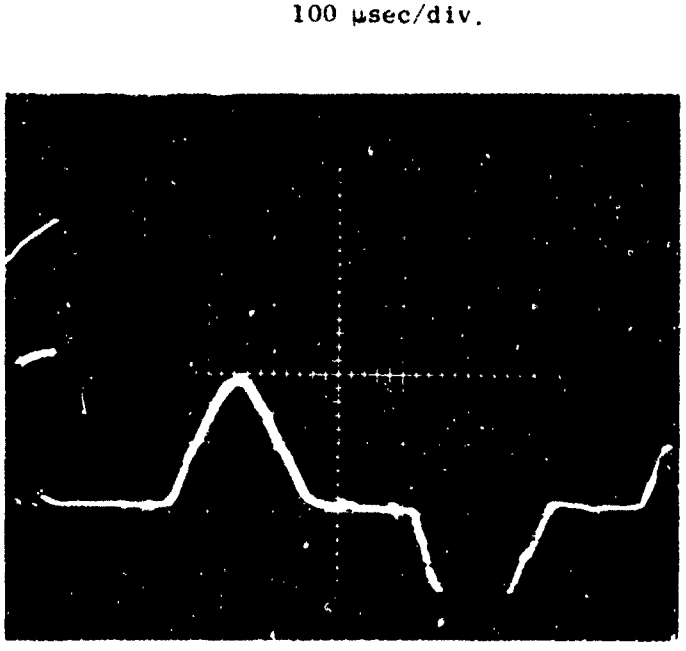

Fig. 30a

100 μsec/div

535 μin/in/div.

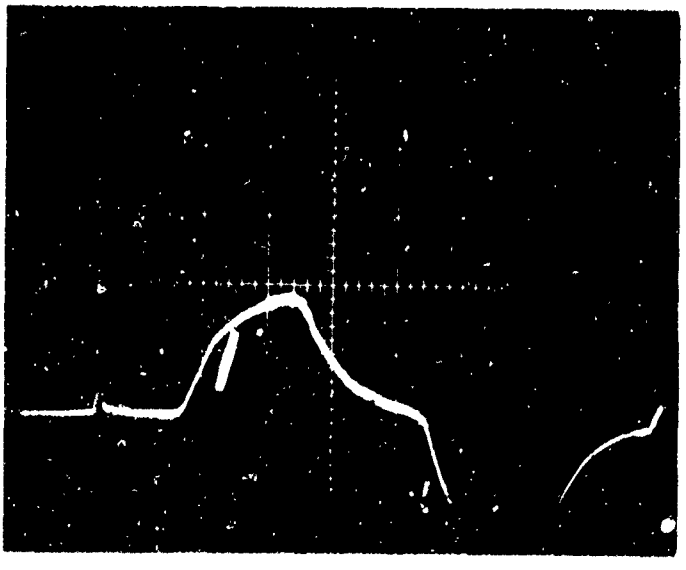

Fig. 30b

BIBLIOGRAPHY

1. Musgrave, M. J. P., "On the Propagation of Elastic Waves in Aeologropic Media; Part 1: General Principles, and Part 2: Media of Hexagonal Symmetry," Proc. Roy. Soc. London, A, Vol. 226, 1954, p. 339 and p. 356.

2. Synge, J. L., "Elastic Waves in Anisotropic Media," J. Math. and Phys., Vol. 35, 1957, p. 323.

3. Synge, J. L., "Flux of Energy for Elastic Waves in Anisotropic Media," Proc. Roy. Irish Acad., Vol. 58, A, 1956, p. 13.

4. Buchwald, V. T., "Elastic Waves in Anisotropic Media," Proc. Roy. Soc. London, A, Vol. 253, 1959, p. 563.

5. Musgrave, M. J. P., "Elastic Waves in Anisotropic Media," Progress in Solid Mechanics, I. N. Sneddon and R. Hill, eds., Vol. 2, North-Holland Publ. Co., Amsterdam, 1961, p. 63.

6. Kraut, E. A., "Advances in the Theory of Anisotropic Elastic Wave Propagation," Rev. Geoph., Vol. 1, 1963, p. 401.

7. Burridge, R., "Lamb's Problem for an Anisotropic Half-Space," Quar. J. Mech. Appl. Math., Vol. 24, Pt. 1, 1971, p. 81.

8. Ricketts, T. E., "Sphere Impact on an Anisotropic Half-Space," Dissertation (Ph.D.), University of California, Berkeley, 1970.

9. Ricketts, T. E., and Goldsmith, W., "Wave Propagation in an Anisotropic Half-Space," submitted to the Int. J. Rock Mech. Min. Sci.

10. Goldsmith, W., Lewis, J. L., and Lewis, Jack L., "Dynamic Fracture of Dry and Wet Cortical Bone," Proc. Third Canadian Cong. Appl. Mech., Calgary, 1971, p. 793.

11. Gurtin, M. E., "The Effects of Accelerometer Low Frequency Response on Transient Measurements," Proc. Soc. Exp. Stress Anal., Vol. 18, 1961, p. 206.

12. Kenner, V. H., and Goldsmith, W., "One-Dimensional Wave Propagation Through a Short Discontinuity," J. Acoust. Soc. Amer., Vol. 45, No. 1, 1969, p. 115.

13. Cunningham, D. M., and Goldsmith, W., "Short-Time Impulses Produced by Longitudinal Impact," Proc. Soc. Exp. Stress Anal., Vol. 16, No. 1, 1959, p. 153.

14. Dove, R. C., and Adams, P. H., Experimental Stress Analysis and Motion Measurement, Columbus, Ohio, C. E. Merrill, 1965.

15. Lion, K. S., Instrumentation in Scientific Research; Electrical Input Transducers, New York, McGraw-Hill, 1959.

16. deHoop, A. T., "A Modification of Cagniard's Method for Solving Seismic Pulse Problems," Appl. Sci. Res., B, Vol. 8, 1960, p. 349.

17. Musgrave, M. J. P., Crystal Acoustics, San Francisco, Holden Day, 1970.

18. Fröberg, C. E., Introduction to Numerical Analysis, 2nd ed. Reading, Mass., Addison Wesley, 1969.

19. Newmark, N. M., "A Method of Computation for Structural Dynamics," Amer. Soc. Civ. Eng., Eng. Mech. Div. Journal, Vol. 85, No. 3, June, 1959

20. Pekeris, C. L., "The Seismic Surface Pulse," Proc. Nat. Acad. Sci. USA, Vol. 41, 1955, p. 469.

21. Bloss, F. D., An Introduction to the Methods o Optical Crystallography, New York, Holt Rinehart and Winston, 1967.